

**MASARYK  
UNIVERSITY**

**FACULTY OF SCIENCE**

**A census of open clusters  
using the Gaia DR3**

**Doctoral Thesis**

**Tahereh Ramezani**

Supervisor: doc. Ernst Paunzen, Dr.rer.nat

Department of Theoretical Physics and Astrophysics

Brno 2025

**DEDICATED TO MY BELOVED  
FATHER AND MOTHER**



# Bibliografický záznam

**Autor:** Tahereh Ramezani  
Přírodovědecká fakulta, Masarykova univerzita  
Ústav teoretické fyziky a astrofyziky

**Název práce:** A Census of Open Clusters Using the Gaia DR3

**Studijní program:** Fyzika

**Specializace:** Astrofyzika

**Vedoucí práce:** doc. Ernst Paunzen, Dr.rer.nat  
Přírodovědecká fakulta, Masarykova univerzita  
Ústav teoretické fyziky a astrofyziky

**Akademický rok:** 2025

**Počet stran:** 63

**Klíčová slova:** Otevřené Hvězdokupy; Gaia; Ultrafialové; Fotometrie

# Bibliographic Entry

**Author:** Tahereh Ramezani  
Faculty of Science, Masaryk University  
Department of Theoretical Physics and Astrophysics

**Title of Thesis:** A Census of Open Clusters Using the Gaia DR3

**Degree Programme:** Physics

**Field of Study:** Astrophysics  
**Supervisor:** doc. Ernst Paunzen, Dr.rer.nat  
Faculty of Science, Masaryk University  
Department of Theoretical Physics and Astrophysics

**Academic Year:** 2025

**Number of Pages:** 63

**Keywords:** Open Clusters; Gaia; Ultraviolet; Photometry

# Abstrakt

Hlavním cílem této práce je pozorovat a analyzovat fotometrická data z neprozkoumaných galaktických otevřených hvězdokup v ultrafialové (UV) oblasti vlnových délek. Nyní můžeme pečlivě prozkoumat známé galaktické otevřené hvězdokupy díky Gaia Data Release 3 (DR3). Pro tyto shluky jsme shromáždili dostupná astrometrická a fotometrická data. Pomocí UV filtrů jsme prováděli pozorování 2.15 metrovým dalekohledem na Complejo Astronómico El Leoncito (CASLEO) v Argentině a 1.54 metrovým dánským dalekohledem (DK1.54) v Chile. Rozsah vlnových délek  $\sim 3650$  (Å) UV je velmi užitečný pro výzkum mezihvězdného zčervenání, které není ovlivněno stářím nebo metalicitou kup. Po pozorování jsme změřili 105 klastrových polí pomocí fotometrie Point Spread Function (PSF). Hvězdy byly poté porovnány s katalogem Gaia Data Release 3. Poté jsme použili naše UV magnitudy a Gaia magnitudy k vytvoření barevně-barevných grafů. Pro každou ze 105 klastrových sekvencí jsme přizpůsobili izochrony. Pro zjištění jejich členství jsme použili katalog Hunt & Reffert (2023). Tato data lze použít k vytvoření prvního homogenního sčítání neprozkoumaných otevřených hvězdokup v Mléčné dráze pomocí ultrafialové fotometrie.

# Abstract

The main goal of this thesis is to observe and analyze photometric data from unexplored Galactic open clusters in the ultraviolet (UV) wavelength region. We can now carefully investigate known Galactic open clusters thanks to Gaia Data Release 3 (DR3). For these clusters, we have gathered the available astrometric and photometric data. Using UV filters, we performed observations with the 2.15-meter telescope at the Complejo Astronómico El Leoncito (CASLEO) in Argentina and the 1.54-meter Danish Telescope (DK1.54) in Chile. The  $\sim 3650$  (Å) UV wavelength range is very helpful for researching interstellar reddening, unaffected by the clusters' age or metallicity. Following the observations, we measured 105 cluster fields using Point Spread Function (PSF) photometry. The stars were then compared to the Gaia Data Release 3 catalogue. We then used our UV magnitudes and Gaia magnitudes to generate color-color graphs. For each of the 105 cluster sequences, we fitted isochrones. We used the Hunt & Reffert (2023) catalogue as a guide to ascertain their membership. These data can be used to create the first homogeneous census of unexplored open clusters in the Milky Way using ultraviolet photometry.

# Acknowledgement

I would like to thank a million from my deep heart to God and my family, especially my beloved father and mother and my nephew, Amin, who always give me hope and motivation. Thanks to my friends from the theoretical department for making me cheerful. I thank my supervisor for his guidance during my study.



# Declaration

I declare that I developed my dissertation independently using information sources that are cited in the work.

Brno 2025

.....

Tahereh Ramezani

# List of Abbreviations

<b>CASLEO</b>	Complejo Astronómico El Leoncito
<b>CCD</b>	Charge-Coupled Device
<b>CMD</b>	Colour-Magnitude Diagram
<b>DR3</b>	Gaia Data Release 3
<b>EDR3</b>	Gaia Early Data Release 3
<b>GAIA</b>	Global Astrometric Interferometer for Astrophysics
<b>IRAF</b>	Image Reduction and Analysis Facility
<b>ISM</b>	Interstellar Medium
<b>NOAO</b>	National Optical Astronomy Observatory
<b>PSF</b>	Point Spread Function
<b>UV</b>	UltraViolet

# List of Related Publications

## Article 1

**Ramezani T.**, Paunzen E., Gorodilov A., Intado O. I. (2025) Ultraviolet Photometry and Reddening Estimation of 105 Galactic Open Clusters. Manuscript accepted. CAOSP Journal.

# List Of Unrelated Publications

## Article 1

**Ramezani T.**, Paunzen E., Piecka M., Kajan M. (2024) A New Approach to Find the Böhm-Vitense gap. Bulgarian Astronomical Journal. Institute of Astronomy and NAO, vol. 41, No 2024, p. 3-18. ISSN 1313-2709.

Available from: <https://dx.doi.org/10.48550/arXiv.2401.09264>.

## Article 2

**Ramezani T.**, Paunzen E., Xia C., Pivonková K., Mondal P. (2024) Estimation of radial velocities of BHB stars. Bulgarian Astronomical Journal. Institute of Astronomy and NAO, vol. 41, No 2024, p. 55-62. ISSN 1313-2709.

Available from: <https://dx.doi.org/10.48550/arXiv.2405.13822>.

## Article 3

Kueß L., Paunzen E., Faltová N., Jadlovský D., Labaj M., Mesarč M., Mondal P., Prišegen M., **Ramezani T.**, Supíková J., Svačinková K., Vítková M., Xia C., Bernhard K., Hümmerich S. (2024) Chemically peculiar stars on the pre-main sequence. Astronomy & Astrophysics. EDP Sciences, vol. 687, July 2024, p. 1-24. ISSN 0004-6361.

Available from: <https://dx.doi.org/10.1051/0004-6361/202348926>.

## Article 4

Faltová N., Jadlovský D., Kueß L., Labaj M., Mesarč M., Mondal, P., Neumannová K., Paunzen E., Prišegen M., **Ramezani T.**, Supíková J., Svačinková K., Szász G., Vítková M., Xia C. (2025) Chemically peculiar stars as members of open clusters. Monthly Notices of the Royal Astronomical Society, Volume 536, Issue 1, pp.72-78, January 2025.

Available from: <https://dx.doi.org/10.1093/mnras/stae2563>.

## Article 5

Krtička J., Benáček J., Budaj J., Korčáková D., Pál A., Piecka M., Zejda M., Bakış V., Brož M., Chang H. K., Faltová N., Gális R., Jadlovský D., Janík J., Kára J., Kolář J., Krtíčková I., Kubát J., Kubátová B., Kurfürst P., Labaj M., Merc J., Mikulášek Z., Münz F., Paunzen E., Prišegen M., **Ramezani T.**, Rieva-jová T., Řípa J., Schmidtbreick L., Skarka M., Szász G., Weiss W., Zajaček M.,

Werner, N. (2024) Science with a Small Two-Band UV-Photometry Mission II: Observations of Stars and Stellar Systems. Space Science Reviews. Springer, vol. 220, No 2, p. 1-34. ISSN 0038-6308, (2024).

Available from: <https://dx.doi.org/10.1007/s11214-024-01058-1>.

## Article 6

Werner N., Řípa J., Münz F., Hroch F., Jelínek M., Krτίčka J., Zajaček M., Topinka M., Dániel V., Gromeš J., Václavík J., Steiger L., Lédl V., Seginak J., Benáček J., Budaj J., Faltová N., Gális R., Jadloviský D., Janík J., Kajan M., Karas V., Korčáková D., Kosiba M., Krτίčková I., Kubát J., Kubátová B., Kurfürst P., Labaj M., Mikulášek Z., Pál A., Paunzen E., Piecka M., Prišegen M., **Ramezani T.**, Skarka M., Szász G., Thöne C., Zejda M. (2022) Quick Ultra-Violet Kilonova surveyor (QUVIK). Proceedings of SPIE, Volume 12181: Space Telescopes and Instrumentation 2022: Ultraviolet to Gamma Ray. Washington: SPIE, 2022, p. 1-7. ISBN 978-1-5106-5343-6.

Available from: <https://dx.doi.org/10.1117/12.2629531>.

## Book 1

Daneshyar M., **Ramezani T.**, Ruhi H. (2023) Determining the time of Friday prayer from an astronomical point of view (in Persian)

# Contents

<b>1</b>	<b>Introduction</b>	<b>14</b>
<b>2</b>	<b>Progress In Knowledge Of Star Clusters In The Gaia Era</b>	<b>15</b>
2.1	Gaia Data Release 1 . . . . .	15
2.2	Gaia Data Release 2 . . . . .	15
2.3	Gaia Early Data Release 3 . . . . .	16
2.4	Gaia Data Release 3 . . . . .	17
2.5	Star Clusters . . . . .	17
2.6	Globular Clusters . . . . .	18
2.7	Open Clusters . . . . .	19
2.7.1	Colour-Magnitude Diagram Of Open Clusters . . . . .	20
2.7.2	The Dynamics Of Open Clusters . . . . .	20
2.7.3	Difference Between Globular Clusters And Open Clusters . . . . .	20
<b>3</b>	<b>Observations Of Open Clusters In The UltraViolet</b>	<b>22</b>
3.1	Photometric Systems . . . . .	22
3.1.1	Purpose Of Photometric Systems . . . . .	22
3.2	Standard Transformations . . . . .	23
3.3	UltraViolet . . . . .	24
3.4	The UV Facilities . . . . .	24
3.5	Instruments . . . . .	25
3.6	DK 1.54 Metre (Danish) Telescope . . . . .	26
3.6.1	Properties . . . . .	28
3.7	Reduction Techniques . . . . .	28
3.7.1	Types Of Reduction Techniques . . . . .	28
3.7.2	IRAF . . . . .	29
3.7.3	PSF Photometry . . . . .	30
3.8	Observation Of Open Clusters In The UltraViolet . . . . .	31
3.8.1	Matching The Observed Stars With Gaia DR3 . . . . .	34
3.8.2	Our Comments For Hunt & Reffert Catalogue . . . . .	34
3.8.3	Colour-Colour Diagrams . . . . .	35
3.8.4	Reddening . . . . .	40
3.9	Estimating The Clusters' Extinction . . . . .	42
<b>4</b>	<b>Summary And Prospects</b>	<b>53</b>
	<b>Bibliography</b>	<b>61</b>

# 1. Introduction

Stars in a cluster have similar ages, distances, and origins, and studying them offers crucial insights into the more extensive processes of stellar development. By analyzing star clusters, we can refine our models of stellar formation and lifecycles, such as those governed by mass, composition, and environment. Studying these clusters in UltraViolet (UV) wavelengths is particularly important because UV observations are sensitive to young, hot, and massive stars. These stars emit most of their light in the UV, making this wavelength regime critical for understanding the early stages of stellar evolution.

One of the key challenges in studying star clusters is interstellar reddening. The light from stars shifts toward redder wavelengths because of the scattering and absorption of starlight by dust grains in the ISM. The location of the star in the Galaxy and the density of the dust column determine the reddening. Accurately calculating star parameters like temperature and luminosities requires accounting for this reddening. Extinction models, such as the Fitzpatrick (1999) model, are commonly used to correct for these effects. These models help to remove the distortion introduced by the ISM and allow us to recover the intrinsic colors and magnitudes of stars.

These data sets have significantly improved our ability to study the hot and young stars that dominate the UV emission of star clusters. Additionally, by cross-matching UV data with optical surveys such as Gaia Data Release 3 (DR3) Gaia Collaboration et al. (2023), we can build color-color diagrams, estimate stellar properties, and correct for reddening with high precision. A comprehensive picture of star populations and their environments can be obtained by combining UV and optical data.

The main objectives of this thesis are to estimate reddening, perform Point Spread Function (PSF) photometric analysis, and observe a broad sample of open star clusters at UV wavelengths. The goal is to understand better how interstellar dust affects star populations by creating colour-colour diagrams and fitting them with the Padova isochrone (Bressan et al. 2012).

# 2. Progress In Knowledge Of Star Clusters In The Gaia Era

## 2.1 Gaia Data Release 1

According to Gaia Collaboration (2016), the presentation of Gaia Data Release 1 (DR1) took place on September 14, 2016. Scientists compiled Gaia DR1, which included photometry and astrometry for almost 1 billion sources brighter than magnitude 20.7, about 1000 days after Gaia’s launch.

Because this publication was still preliminary, scientists discussed the data’s limitations after providing an overview of its scientific quality.

In addition to a secondary set of astrometric data that includes the positions of an additional 1.1 billion sources, Gaia DR1 also included a primary astrometric data set that contained the positions, parallaxes, and mean proper motions of about 2 million of the brightest stars that were also in the Hipparcos and Tycho-2 catalogues.

The photometric data collection, which included the average G-band magnitudes for every source, was the second element. G-band light curves and features of around  $\sim 3000$  Cepheid and RR Lyrae stars that were detected at a high cadence around the south ecliptic pole were included in the third component. For the core astrometric data collection, the mean uncertainty was roughly one mas/yr for the proper motions and 0.3 mas for the locations and parallaxes. It is necessary to include a systematic  $\sim 0.3$  mas component in the parallax uncertainty.

The proper motions for the subset of  $\sim 94000$  Hipparcos stars in the core data set were substantially more accurate at about 0.6 mas/yr. The secondary astrometric data set had an average position uncertainty of  $\sim 10$  mas.

The median uncertainty on the mean G-band magnitudes was between  $\sim 0.03$  mag and the mili-mag level for the magnitude range of 5 to 20.7.

The availability of original stellar data, which is the foundation of observational astrophysics, and the mapping of the skies were both significantly advanced by Gaia DR1.

However, because of the extremely early nature of this first Gaia data release, some significant data quality issues arose that should be thoroughly addressed before making any inferences (Gaia Collaboration et al. 2016).

## 2.2 Gaia Data Release 2

It includes data on astrophysical parameters, photometry, radial velocity, astronomical observations, and variability of objects brighter than magnitude 21.

Moreover, photometry, astronomical data, and epochs are given for a small sampling of the solar system’s smaller planets.

A summary of Gaia DR2’s material was given, along with an explanation of how it differs from Gaia DR1 and the primary constraints that the study still has.



The responsible use of Gaia DR2 results has been recommended (Gaia Collaboration et al. 2018).

This second data release (Monti et al. 2024) is the result of the Gaia Data Processing and Analysis Consortium (DPAC) processing the raw data that Gaia instruments collected over the first 22 months of the mission (Brown et al. 2018).

The Gaia Collaboration claims that notable improvements in the completeness, performance, and richness of data products were achieved compared to Gaia DR1.

Sky locations and apparent magnitudes ( $G$ ) for roughly 1.7 billion sources were included in Gaia DR2.

Parallax and eigenmotion were also available for 1.3 billion of these sources.

They have increased the number of sources that provide variability information to 500,000 stars. There are four new components in this data release.

1.4 billion light sources now have access to 4444 broadband color information in the form of perceived brightness in the  $G_{BP}$  (330-680 nm) and  $G_{RP}$  (630-1050 nm) bands.

It showed the average radial velocity of almost 7 million sources and estimated the star radius, brightness, redness, extinction, and effective temperature.

Additionally, photometric and astronomical data were provided for a pre-selected selection of 14,000 solar system asteroids.

Last, Gaia DR2 is a new optical representation of the celestial reference frame, Gaia-CRF2.

It is the first optical reference frame solely obtained from extragalactic light sources.

The long-standing goal of delivering parallax and motion-appropriate motion for over a billion stars, as well as supplementary radial velocity and astrophysical analysis for a sample of stars, is fulfilled by Gaia DR2, a notable mission outcome.

It was the initial stage of making source information available.

A crucial portion of the volume of our galaxy is covered by the Gaia study (Gaia Collaboration et al. 2018).

## 2.3 Gaia Early Data Release 3

According to Gaia Collaboration (2021), sky locations and apparent magnitudes ( $G$ ) for roughly 1.8 billion sources were included in Gaia EDR3.

Additionally, parallax, intrinsic motion, and  $(G_{BP} - G_{RP})$  color were accessible for 1.5 billion of these sources.

The publication contained passbands for  $G$ ,  $G_{BP}$ , and  $G_{RP}$ .

After reducing specific noise values, this version incorporates the 7 million radial velocities of Gaia DR2 for convenience.

The Gaia DR3 includes the updated radial velocity.

Lastly, Gaia EDR3 was an upgraded instantiation of the celestial reference frame (CRF) based only on extragalactic sources within Gaia optical CRF3.

The source list for Gaia EDR3 was improved to be more resilient to the destructive impacts of cluster and partially resolved sources as well as stars with high proper motions.

Although there were some significant changes and new sources, the source list was almost the same as that of Gaia DR2. The list of sources for Gaia DR3 has not changed.

Gaia EDR3 reduces systematic errors in astronomical surveys by 30–40 % for parallax and a factor of  $\sim 2.5$  for correct operation; it also improves self-motion accuracy by two times and parallax accuracy by 30%.

Better accuracy and, most importantly, significantly better color, brightness, and sky position consistency are characteristics of photometry.

With no bias above the 1% threshold, the single passbands of  $G$ ,  $G_{BP}$ , and  $G_{RP}$  were valid across the whole brightness and color spectrum (Gaia Collaboration et al. 2021).

## 2.4 Gaia Data Release 3

During the first 34 months of the mission, the Gaia Data Processing and Analysis Consortium (DPAC) collected raw data using Gaia sensors, which were then processed to produce the Gaia DR3 database.

As in its third data release, the Gaia DR3 catalogue contains the source list, sky position, proper motion, parallax, and broadband photometry in the  $G$ ,  $G_{BP}$ , and  $G_{RP}$  passbands.

Gaia DR3 offers a staggering array of new data products. The Radial Velocity Spectrometer (RVS) of over 33 million objects in the  $RVS < 14$  (km/s) and  $3100$  (K)  $< T_{eff} < 14500$  (K) may be determined using data gathered by Gaia. The researcher specified the line width expansion parameters for a subset and gave its RVS sizes for the majority of radial velocity sources. About 1 million average spectra from the radial velocity spectrometer and about 220 million from the low-resolution blue and red prism photometers BP and RP were included in the Gaia DR3 catalogue. Results of epoch photometric analysis were presented for roughly 10 million light sources with 24 different types of variations.

Astrophysical parameters and source class probabilities for roughly 470 million and 1.5 billion sources, such as stars, galaxies, and quasars, are available in Gaia DR3. About 800,000 astronomical, spectroscopic, and eclipsing binaries were given orbital elements and trend characteristics. Over 150,000 solar system objects, discoveries, early orbital analyses, and observations from a single period are included in this article. For over 60,000 asteroids, reflectance spectra derived from epoch BP and RP spectral data are publically accessible (Gaia Collaboration et al. 2023).

## 2.5 Star Clusters

Star clusters are groups of physically related stars bound together by their gravitational source. Over a period of a few million years, every member of a star cluster is born within one Giant Molecular Cloud (GMC) <sup>1</sup>. The primary characteristics of each member of a distinct star cluster are: 1) Reddening, 2) Age, 3) Distance, and 4) Metallicity.

---

<sup>1</sup><http://stellar-journeys.org/OpenCluster-Tour.htm>

Each member of a distinct star cluster possesses:

- Identical distance from the Sun: +- The volume expansion of the cluster (diameters  $< 25$  pc)
- Identical age: +- Time scale of star formation (a few Myrs)
- Identical metallicity: +- Inhomogeneities of the initial GMC and the chemical evolution of the giant branch
- Identical kinematical characteristics (radial velocity and proper motion): +- Intrinsic spread

## 2.6 Globular Clusters

Globular clusters are groups of stars that are bound together by the force of gravity. The number of individual stars in these clusters can range from tens of thousands to millions, with a higher stellar density in the center regions.

According to Bastian & Lardo (2018), globular clusters can be found in almost all galaxies. Spiral galaxies like our Milky Way are predominantly located in the more numerous Globulars in the Galactic Bulge. These clusters are the largest and most massive type of star cluster, typically older, denser, and containing lower amounts of heavy elements than open clusters, usually situated in spiral Galaxies disks. Traditionally, globular clusters have been described as a population of stars originating from a single massive cloud of gas and dust, resulting in a uniform age and metallicity (the proportion of heavy elements in their composition). However, modern observations indicate that nearly all globular clusters possess multiple stellar populations (Bastian & Lardo 2018).

According to Burkert & Tremaine (2010), the stars in globular clusters come mostly from places with higher interstellar gas density and more efficient star formation than those seen in other star-forming regions. Globular cluster development is common in starburst zones and interacting galaxies. The size of the globular cluster systems in elliptical and lenticular galaxies is correlated with the mass of the supermassive black holes at their centers. In these galaxies, the mass of the supermassive black hole is frequently comparable to the total mass of the galaxy's globular clusters (Burkert & Tremaine 2010).

According to Gratton et al. (2019), globular clusters usually comprise hundreds of thousands of old stars with low metallicity. These stars resemble those found in the central bulge of a spiral galaxy. Still, they are confined within a spheroidal structure, emitting half of their light within a radius ranging from a few to several tens of parsecs (Gratton et al. 2019).

According to Leonard (1989), as globular clusters have a high stellar density, close contacts and near-collisions between stars are common. Different star classes, such as blue stragglers are produced by these unintentional collisions and are more commonly observed in globular clusters. The exact formation mechanism of blue stragglers remains uncertain. Still, prevailing models suggest interactions between stars, including stellar mergers, mass transfer between stars, or even encounters between binary star systems (Leonard 1989).

## 2.7 Open Clusters

According to Payne-Gaposchkin (1979), an open cluster consists of a few thousand stars formed from the same massive cloud of gas and dust and possess similar ages. Open clusters are crucial in studying various aspects of astrophysics, including star formation, stellar evolution, Galactic kinematics, and dynamics. These clusters are only found in spiral and irregular galaxies where active star formation is ongoing (Payne-Gaposchkin 1979).

According to Lada (2010), this collapsed portion of the cloud will progressively fragment into ever-diminishing clusters, including a dense subtype known as infrared dark clouds, which will ultimately give rise to thousands of stars. This star's formation occurs inside the collapsing cloud's shell.

An HII region will form as a result of the newly formed stars with the highest temperatures and most extraordinary masses, known as OB stars, emitting a strong and constant stream of ultraviolet radiation that gradually ionizes the nearby gaseous matter of the massive molecular cloud. The ionized gas will then be ejected from the gaseous medium at a speed that mirrors sound due to the radiation pressure and stellar winds of the big stars. The cluster will see its first core-collapse supernovae after a few million years, driving the gas out of the local area. Within ten million years, these activities will often exhaust the cluster's gaseous composition, preventing additional star formation cycles. However, about half of the resulting protostellar objects will survive, surrounded by circumstellar disks, many of which take the shape of accretion disks (Lada 2010).

According to Shu et al. (1987), during the pre-collapse phase, these clouds use rotation, turbulence, and magnetic fields to maintain their mechanical equilibrium. A massive molecular cloud can be disturbed by several things, leading to a collapse and the subsequent explosion of star formation that eventually results in an open cluster. These elements include gravitational pull, collisions with other clouds, or shock waves from a nearby supernova. Notably, areas of the cloud can develop the circumstances necessary for instability and eventual collapse even in the absence of external influences (Shu et al. 1987).

According to Hills (1980), many open clusters are intrinsically unstable as the mass of the pre-collapse stage is below the threshold required to exceed the average velocity of the individual stars and allow escape. These clusters will, therefore, quickly spread out over a few million years. Frequently, the stripping away of the gas from which the cluster originated, resulting from the radiation pressure exerted by the youthful and fervent stars, will sufficiently diminish the cluster's mass, thereby expediting its dispersal (Hills 1980).

According to Archinal & Hynes (2003), open clusters are instrumental in determining the structure of galaxies. Because their bright components allow for examination from a great distance, their distance may be calculated more precisely than that of a single star. Furthermore, because they are relatively young, they are perfect indicators for the newest part of the galactic disk (Archinal & Hynes 2003).

Depending on the age, the open clusters can be classified into three groups: (Sung et al. 2013)

- young (age  $\lesssim 10^7$  yrs)

- intermediate-age (age:  $10^7 - 7 \times 10^8$  yrs)
- old (age  $\gtrsim 7 \times 10^8$  yrs)

### 2.7.1 Colour-Magnitude Diagram Of Open Clusters

According to Archinal & Hynes (2003), due to the relative youth of numerous open clusters, it would be reasonable to anticipate that a substantial proportion of the constituent stars will be situated in the main sequence (the segment of the color-magnitude diagram where the majority of stars reside during the typical hydrogen-burning stage of their evolution). This assumption is valid for the most part. A reasonably well-defined band contains the majority of cluster stars. Some open clusters have remained together for extended periods and are no longer young; a few could be as old as the disk of the Milky Way. A notable presence of red giants distinguishes these clusters. The age of a cluster can be estimated by examining the colour and the luminosity of the main-sequence turn-off point (Archinal & Hynes 2003).

### 2.7.2 The Dynamics Of Open Clusters

According to Archinal & Hynes (2003), uncertainty may be most significant in studying open cluster dynamics. This is mainly because each object has a minimal number of stars, and the computations become more complex as the number of stars declines.

In addition to the motions of the open cluster members within the cluster (resulting from their mutual gravitational interactions), several additional elements can significantly impact its dynamics. During the cluster's orbit around the Galaxy's centre, it is unavoidable to encounter field stars; these interactions impact the velocity distribution of stars within the cluster, mainly if the cluster passes through an area densely populated with massive stars. The galactic tidal forces also shape the clusters' size, which removes less gravitationally bound stars. Additionally, the tidal effects from the presence of massive molecular clouds contribute to this phenomenon (Archinal & Hynes 2003).

### 2.7.3 Difference Between Globular Clusters And Open Clusters

The Milky Way's star clusters have the following characteristics:

	<b>Open Clusters</b>	<b>Globular Clusters</b>
<b>Age</b>	$< 5$ Gyr	$\leq$ age of the Milky Way
<b>Distance from the Sun</b>	$> 45$ pc	$> 2000$ pc
<b>Mass range of the members</b>	Complete range depending on the age of the cluster	$< 20 M_{\odot}$
<b>Total mass</b>	$< 60\,000 M_{\odot}$	$< 1\,000\,000 M_{\odot}$
<b>Absolute diameter</b>	$< 25$ pc	$< 100$ pc
<b>Metallicity</b>	-1.0 to +0.6 dex compared to the Sun	-2.5 to -0.5 dex compared to the Sun
	Main-sequence (MS) turn-off point varies massively, faintest is consistent	MS turn-off points in similar position. Giant branch joining MS
	Maximum luminosity of stars can get to $M_v \approx -10$ mag	Horizontal branch from giant branch to above the MS turn-off point with globulars
	Very massive stars found in these clusters	Horizontal branch often populated only with variable RR Lyrae stars

The differences are interpreted due to age. Open clusters lie in the disk of the Milky Way and have an extensive range of ages. The oldest known objects are the globulars, which date back to the early phases of the Milky Way's development ( $\sim 12 \times 10^9$  yrs) (Stetson et al. 1996).

# 3. Observations Of Open Clusters In The UltraViolet

## 3.1 Photometric Systems

Photometric systems are frameworks used to measure and compare the brightness of astronomical objects through different filters or wavelength bands. They allow astronomers to quantify the flux of light received from a star or other celestial object in specific spectral regions, enabling comparison across different observations and studies.

Photometric systems are categorized based on the number of filters and the spectral regions they cover. The most common types are:

- **Broadband Systems:** These systems use broad filters that cover wide spectral regions (e.g., ultraviolet, visible, infrared). Examples include:
  - **UBV System:** One of the first standard systems developed by Johnson and Morgan (1953), it uses three filters: U (ultraviolet), B (blue), and V (visual) (Johnson & Morgan 1953).
  - **Sloan Digital Sky Survey (SDSS):** This system covers five broadband filters (u, g, r, i, z) ranging from the near-ultraviolet to the near-infrared (Fukugita et al. 1996).
  - **Gaia Photometric System:** Gaia photometric contains G-band photometry, and the  $G_{BP}$  and  $G_{RP}$  photometry from the integration of the blue and red photometer (BP and RP) low-resolution spectra (Gaia Collaboration et al. 2018).
- **Narrowband Systems:** Narrowband systems use filters that cover particular, narrow ranges of wavelengths, often focusing on particular spectral lines (e.g.,  $H\alpha$ ,  $O[III]$ ), like: **Strömgren System:** This system uses four narrow filters (u, v, b, y) to study stars' temperature, metallicity, and surface gravity (Strömgren 1966).
- **Intermediate-band Systems:** These systems utilize intermediate width filters between broadband and narrowband systems. An example is the Washington system, designed to study stars' metallicities (Canterna 1976).

### 3.1.1 Purpose Of Photometric Systems

Photometric systems have some important purposes in astronomy:

- **Determining Distance:** Using standard candles like Cepheid variables or Type Ia supernovae, photometric measurements can help determine distances to stars and galaxies.
- **Stellar Population Studies:** By observing galaxies and star clusters in different photometric bands, astronomers can infer information about the age, metallicity, and star formation history of stellar populations (Bessell 2005).

Photometric systems are fundamental tools in observational astronomy, allowing researchers to systematically study the properties of celestial objects across different wavelengths.

## 3.2 Standard Transformations

There are various uses for photometric systems in astronomy:

- **Classifying Stars:** Astronomers can categorize stars based on their temperature, brightness, and metallicity by comparing data from various filters.
- **Measuring Reddening and Extinction:** Observations in multiple photometric bands can be used to assess the effects of interstellar dust, which causes reddening and extinction of light.

In observational astronomy, photometric systems are essential instruments that enable scientists to examine the characteristics of celestial objects at various wavelengths methodically.

To maintain consistency across several datasets or telescopes, standard transformations are equations or processes that translate data from one observational system or filter set (photometric or spectroscopic) to another.

These transformations are significant in astronomy, where other instruments and observatories may use different photometric systems, resulting in the need to standardize observations for comparison.

Examples of standard transformations in astronomy are:

- **Photometric Transformations: Johnson-Cousins System:** Converting between the Johnson-Cousins UBVRI system and other filtering systems, such as Gaia or SDSS. For example, standard adjustments based on color equations and empirical connections are required when converting from SDSS magnitudes (u, g, r, i, z) to Johnson-Cousins (B, V).
- **Gaia Transformations:** To compare data from other surveys, Gaia magnitudes (G, BP, RP) are converted to other photometric systems, such as Johnson, 2MASS, etc.
- **Spectroscopic Transformations: Velocity Transformations:** Converting observed velocities to heliocentric velocities, accounting for Earth's motion relative to the Sun.
- **Metallicity Transformations:** Transforming metallicity measurements from one scale (e.g.,  $[\text{Fe}/\text{H}]$  in different surveys) to a standardized scale for comparison.
- **colour Transformations:** Standardizing the colours of stars, galaxies, and other astronomical objects by converting colour indices (such as (B-V) to (g-r)) between various photometric systems.
- **Coordinate Transformations:** Coordinate transformations include converting equinoxes or reference frames (e.g., from B1950 to J2000) into celestial coordinates (RA, Dec).



### 3.3 UltraViolet

The UltraViolet (UV) cosmos is very different from the familiar stars and galaxies visible to the naked eye.

Measurements of the ultraviolet spectrum are used to determine the chemical composition and properties of the interstellar medium, as well as the temperature and composition of hot newborn stars.

Important details regarding the evolution of galaxies can also be obtained from ultraviolet measurements.

These can detect the presence of hot white dwarfs or main sequence companion stars orbiting more fabulous stars. Ultraviolet light helps researchers track the bright glow of young blue star clusters in galaxies. The study of electromagnetic radiation at ultraviolet wavelengths, which range from around 10 to 320 nanometers, is known as UV astronomy. The study of shorter wavelengths, which correlate to higher-energy photons, is the main emphasis of X-ray and gamma-ray astronomy. The majority of light at ultraviolet wavelengths is absorbed by the Earth's atmosphere, therefore observations in this range must be made from space or the high atmosphere (ClabonWalter & Cox 2000).

### 3.4 The UV Facilities

Some astronomical satellites are working in the UV range:

- The Hubble Space Telescope (HST)
- The Galaxy Evolution Explorer (GALEX)
- Far Ultraviolet Spectroscopic Explorer (FUSE)
- The World Space Observatory - Ultraviolet (WSO/UV)
- Microsatellite à Traînée Variable Expérimental (MAUVE)
- Quick Ultra-Violet Kilonova surveyor (QUVIK)

According to Gómezde castro & Wamsteker (2004), the Hubble Space Telescope (HST) and the Far Ultraviolet Spectroscopic Explorer (FUSE) are both observatory missions that contribute to the field of ultraviolet astronomy. Furthermore, the Galaxy Evolution Explorer (GALEX) primarily focuses on conducting the first comprehensive all-sky ultraviolet survey.

Additionally, a specialized sky survey called TAUVE, which is specifically oriented towards interstellar absorption, was launched in 2005 through a collaboration between the Indian Space Research Organisation (ISRO) and the International Space Astrophysics Laboratory (ISA)(Gómez de Castro & Wamsteker 2004)

MAUVE is a satellite-mounted instrument equipped with a 13 cm telescope and a UV-visible spectrometer (operational from 200-700 nm) developed with primarily repetitive applications for assessing stellar magnetic activity and variations. The launch of MAUVE's mission is planned for October 2025, and its duration is set for 3 years with an ambition of 5 years. It will encompass a broad

field of regard of  $-46.4$  to  $31.8$  degrees in ICRS during this period. This facility was designed to allow for pilot studies and creative science, and it is entirely for time dome astronomy. The principal surveys to be carried out by MAUVE include lengthy baseline investigations of flare stars, hush-bride Ae/Be stars, host begin exoplanets, and binary variable contact binaries (rs cvn variables, symbiotic stars, liquefaction-type stars, etc. along these other kick employers). Apart from these primary objectives, the MAUVE's most advanced spectrometer has various advantages targeting telescope, which can promote new or current devices by selling new devices (Majidi et al. 2024).

Future wide-field multi-wavelength surveys and the possibility of finding gravitational wave observatories will both benefit from QUVIK's capabilities. Measuring the evolution of the UV brightness of kilonovae, which are produced when two neutron stars merge, is the main goal of the expedition. This will assist in distinguishing between the various explosion scenarios. After a few years, this mission is anticipated to launch as a follow-up to the Ultraviolet Transient Astronomy Satellite (ULTRASAT). Additionally, it will have exceptional and distinctive capabilities for tracking other transients at both near and far ultraviolet wavelengths. It is anticipated to launch anytime after 2028, most likely in 2030. (Werner et al. 2024)

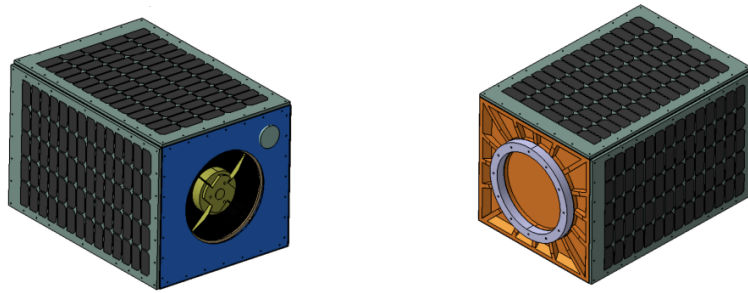


Figure 3.1: Two different perspectives of the QUVIK micro-satellite that accommodates a near-UV space telescope. (Werner et al. 2022)

### 3.5 Instruments

According to Kerr (2005), spectral measurements of solar UltraViolet (UV) radiation have been conducted at various ground-based locations for over 10 years at specific sites. These measurements hold significance for two primary reasons. Firstly, when combined with the outcomes of radiative transfer models, the measurements contribute to our comprehension of the numerous intricate radiative transfer processes occurring in the atmosphere and at the Earth's surface.

In these processes, radiation is absorbed by environmental gases, like sulfur dioxide and ozone, scattered by clouds and aerosols in the atmosphere, and scattered off the Earth's surface. Understanding these procedures is necessary for practical applications like forecasting the UV index and calculating surface UV radiation from satellite data.

Accurately forecasting UV climatology in the past and the future also requires a thorough grasp of the UV radiative transfer processes. The second justification for doing routine ground-based UV radiation observations is to determine whether

any long-term changes occur due to climate change or ozone depletion and to pinpoint the precise causes.

Instances demonstrating how long-term ground-based data records have contributed to our comprehension of surface UV radiation are presented (Kerr 2005).

### 3.6 DK 1.54 Metre (Danish) Telescope

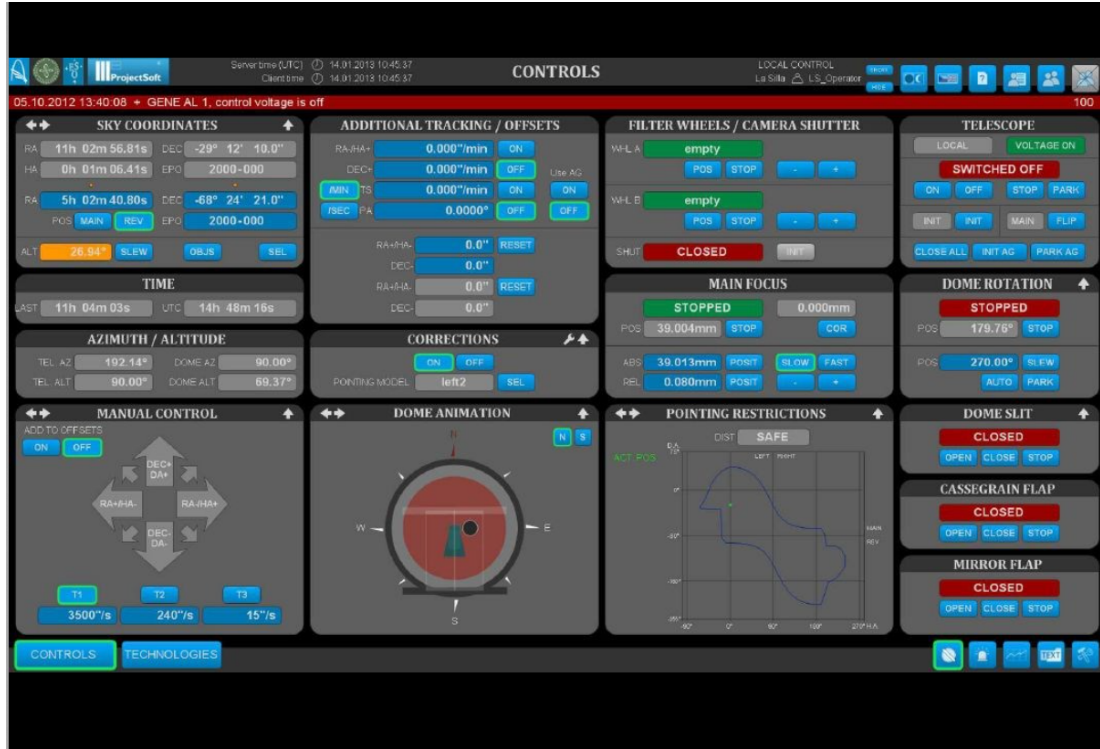


Figure 3.2: Control page of the DK 1.54 Metre (Danish) telescope. (Andersen 2019)

According to Andersen (2019), it was established in 1969. The owner of the building is the University of Copenhagen (ESO possesses the building). It was jointly operated by NBI and research groups in the Czech Republic, with support from ESO. In 1986, an entirely digitally controlled system was installed. An integrated 6-channel photometer, u, v, b, y -  $H_{\beta}$  photometer (Strömgren-photometry), which yields spectral type, luminosity class, and abundance, was incorporated into the control system (Andersen 2019).

- Main mirror is 1.54 meters
- It has an optical system classical Ritchey-Chrétien
- It has Zervit (Zerodur) mirrors
- It has a focal length of  $\sim 13$  meters
- It has an Equatorial (German) mount (Andersen 2019)

<b>Name</b>	Danish 1.54 metre telescope
<b>Location</b>	La Silla
<b>Altitude</b>	2375 m
<b>Enclosure</b>	Classical dome
<b>Optical design</b>	Design: Ritchey-Chrétien Reflector
<b>Diameter. Primary M1</b>	1.54 m
<b>Material. Primary M1</b>	Cervit
<b>Diameter. Secondary M2</b>	0.61 m
<b>Material. Secondary M2</b>	Cervit
<b>Mount</b>	Off-axis equatorial mount
<b>First light date</b>	20 November 1978
<b>Science goal</b>	Photometry, Stellar populations, Comets, Spectroscopy of galaxies and QSO's, Elliptical galaxies
<b>Consortium</b>	Niels Bohr Institute (Denmark) with funding from the Carlsberg Foundation

The El Leoncito Astronomical Complex (Complejo Astronómico El Leoncito - CASLEO) is an astronomical observatory in the San Juan Province of Argentina. CASLEO is one of two El Leoncito National Park observatories that experience minimal cloud cover. The other facility present in the park is the Carlos U. Cesco Astronomical Station of the Félix Aguilar Observatory.

In 1983, CASLEO was created by an agreement between Argentina's National Scientific and Technical Research Council (CONICET) <sup>1</sup>, the Ministry of Science, Technology and Innovation (MINCYT) <sup>2</sup> of Argentina, the National University of San Juan (UNSJ) Cárdenas et al. (2023), the National University of La Plata (UNLP), and the National University of Córdoba (UNC). The facility was officially inaugurated in 1986, and regular observations commenced in 1987.

According to Aballay (2019), all the telescopes at CASLEO and their instruments are fully automated and routinely operated remotely. Observers can utilize the 2.15 m Jorge Sahade Telescope (JST) for imaging, CCD polarimetry, and spectroscopy (both low and high resolution), with future instrumental advancements currently in progress. The Helen Sawyer Hogg (HSH) 0.6 m telescope

<sup>1</sup><https://web.archive.org/web/20111215230227/casleo.gov.ar/visita-en.php>

<sup>2</sup><https://fundit.fr/en/institutions/ministry-science-technology-and-productive-innovation-argentina-mincyt>

is now also accessible for remote observation and can be employed to capture images with an arcmin field of view. Additionally, two smaller telescopes, operated under agreements with NCAC (Poland) and IAA (Spain), are operational at CASLEO. The Argentine community has 20% access to the available time at each instrument, although solely in service mode (Aballay et al. 2019).

### 3.6.1 Properties

<b>Name</b>	Complejo Astronomico El Leoncito (CASLEO)
<b>Location</b>	San Juan Province, Argentina
<b>Altitude</b>	2.483 metres (8.146 ft)
<b>Established</b>	1983
<b>Coordinates</b>	31.7986° <i>S</i> , 69.2956° <i>W</i>
<b>Observatory Code</b>	829
<b>Organization</b>	National Scientific and Technical Research Council

## 3.7 Reduction Techniques

The processes and approaches employed for converting raw observational data into a format suited to scientific analysis are known as reduction techniques in astronomy. Such techniques are critical when attempting to remove noise, modify for instrumental effects, and ensure that the measurements correctly indicate the features of the detected astronomical resources.

Data reduction is a crucial step in both photometric and spectroscopic analysis, and it is widely used in ground-based and space-based observations.

### 3.7.1 Types Of Reduction Techniques

Reduction techniques can vary depending on the type of observation (e.g., imaging, spectroscopy), the instrument used, and the analysis goals.

According to Grisetti (2006), cleaning the images to make them suitable for scientific study is the aim of the reduction procedure. By removing noise from outside sources, this approach produces rectified images that align with our research aims and may be used for analysis (Grisetti 2006).

Typical reduction methods include:

**Bias Subtraction:** This step removes the electronic bias signal the detector introduces when it receives no light. A bias frame, a zero-exposure image, is subtracted from all science frames.

**Dark Subtraction:** Dark frames are taken with the same exposure time as the science images but with the shutter closed, capturing the thermal noise of the detector. These dark frames are subtracted from the science frames to remove this noise.

**Flat-Field Correction:** This process corrects for variations in pixel sensitivity across the detector and uneven illumination of the detector due to vignetting or dust. A flat-field image, typically taken by observing a uniformly illuminated source, normalizes the science frames (Howell 2006).

**Cosmic Ray Removal:** High-energy cosmic rays can hit the detector and leave unwanted bright spots in the images. Techniques such as median combining

multiple frames or algorithms designed to detect and remove cosmic ray hits are employed to clean the data.

**Sky Subtraction:** Especially important in ground-based observations, sky subtraction removes the Earth’s atmosphere’s contribution, adding background light to the observed images. This is done by taking sky frames (images of the empty sky) and subtracting them from the science frames (Horne 1986).

**Wavelength Calibration (for Spectroscopy):** Wavelength calibration involves assigning accurate wavelengths to the pixel positions in a spectrum. This is done using comparison lamps, which produce emission lines at known wavelengths (e.g., Th-Ar, Ne).

**Flux Calibration:** In photometry, flux calibration converts instrumental magnitudes to physical fluxes by observing standard stars with known magnitudes and comparing them to the science targets. In spectroscopy, this step corrects for the instrument’s response as a function of wavelength (Bessell 2005).

**Image Stacking and Combination:** Several exposures are sometimes combined to improve the signal-to-noise ratio and eliminate transitory distortions like cosmic rays. Averaging, median-combining, or advanced techniques like drizzle may be employed to accomplish this (Fruchter & Hook 2002).

**Astrometric Calibration:** To guarantee precise object positional measurements, this procedure aligns the photos with recognized celestial coordinate systems. It entails adjusting for aberrations and matching the image’s stars to their catalogue locations (Calabretta & Greisen 2002).

**Photometric Calibration:** It involves converting instrumental magnitudes to a standard system (e.g., UBV, SDSS) by observing standard stars and applying zero-point corrections to the science data (Stetson 1987).

Reduction techniques are essential for converting raw observational data into scientifically sound information. They ensure that the final measurements reflect the actual properties of the astronomical objects, free from instrumental or environmental distortions.

### 3.7.2 IRAF

According to Tody (1986), The National Optical Astronomy Observatory (NOAO), run by the association of universities for astronomy research, produced the Image Reduction and Analysis Facility (IRAF), a software compilation. Its main function is to reduce astronomical pictures and spectra, which are mostly acquired from imaging array detectors such as CCDs, into pixel array form. IRAF offers cross-platform support for VMS and UNIX-like systems and is compatible with all primary desktop and mainframe operating systems. IRAF can now be used with the Windows Subsystem for Linux, even though Cygwin made it easier to use on previous iterations of Microsoft Windows. Presently, IRAF is primarily employed on macOS and Linux platforms (Tody 1986).

IRAF utilizes a structure of organized commands called tasks, which are grouped into package structures. Additional packages can be incorporated into IRAF, some of which may contain others. NOAO provides numerous packages, and external developers often contribute packages that focus on specific areas of research or facilities.

IRAF’s capabilities include adjusting the fluxes and locations of astronomical

objects in an image, correcting for sensitivity differences between detector pixels, combining multiple images, and determining the redshifts of absorption or emission lines in a spectrum.

Although IRAF remains highly popular among astronomers, its institutional development and maintenance have ceased. However, it continues to be maintained as community software.

### 3.7.3 PSF Photometry

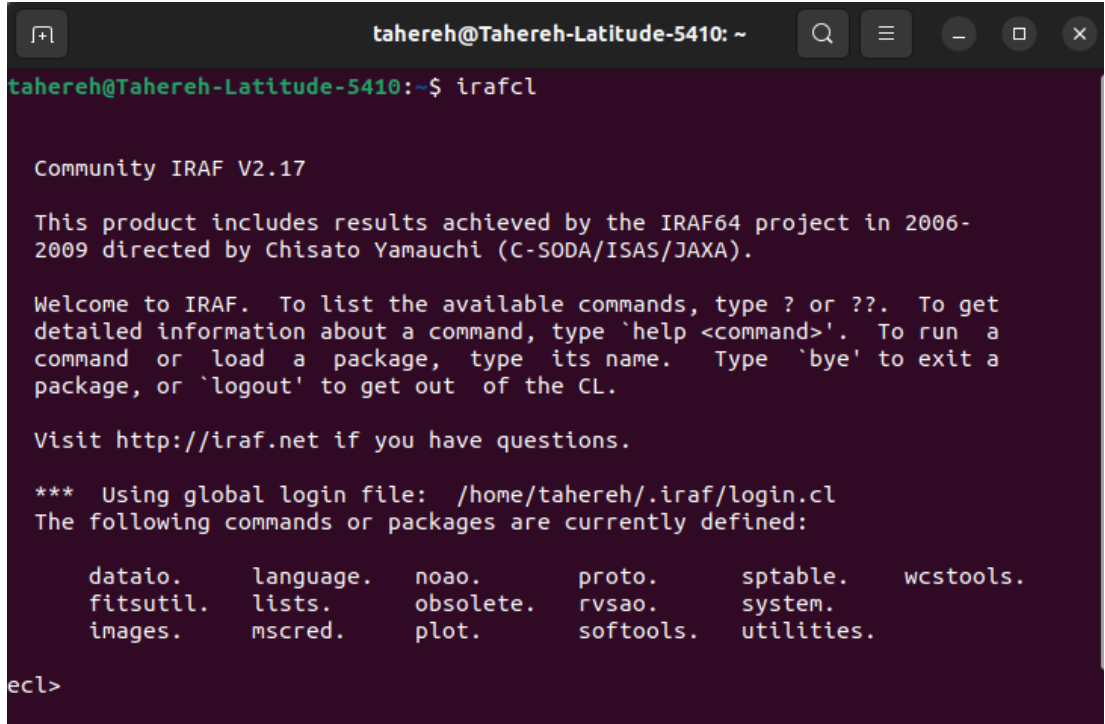
According to Heasley (1999), Point Spread Function (PSF) fitting Photometry has

proven to be a valuable technique for determining the magnitudes of stars in crowded fields. This overview focuses on the fundamentals of PSF fitting photometry, intended for new and potential users. It emphasizes the standard practices shared by most programs developed for this purpose.

In cases where there is a very bright star within or near our cluster, the PSF is compromised. Thus, it is necessary to remove this saturated star to restore a reliable PSF. This star lacks a measurable magnitude.

During the execution of PSF photometry, two fundamental assumptions are made:

- A point spread function can represent all point sources captured by the atmosphere-telescope-detector system. If this function lacks spatial invariance, we assume it is ascertainable and can be modeled.
- The imaging system exhibits linearity in its response to input radiation. Observers must be aware of the limitations of their detector systems (Heasley 1999).



```
tahereh@Tahereh-Latitude-5410:~$ irafcl

Community IRAF V2.17

This product includes results achieved by the IRAF64 project in 2006-
2009 directed by Chisato Yamauchi (C-SODA/ISAS/JAXA).

Welcome to IRAF. To list the available commands, type ? or ??. To get
detailed information about a command, type 'help <command>'. To run a
command or load a package, type its name. Type 'bye' to exit a
package, or 'logout' to get out of the CL.

Visit http://iraf.net if you have questions.

*** Using global login file: /home/tahereh/.iraf/login.cl
The following commands or packages are currently defined:

      dataio.      language.      noao.      proto.      sptable.      wcstools.
      fitsutil.    lists.      obsolete.  rvsao.      system.
      images.      mscred.    plot.      softtools.  utilities.

ecl>
```

Figure 3.3: IRAF

## 3.8 Observation Of Open Clusters In The UltraViolet

We observed 105 open clusters in the ultraviolet filter since it is the most accurate method of identifying reddening. Reddening is independent of metallicity and age. We use isochrone fitting as our technique. Reddening is required for isochrone fitting. We made observations using a CASLEO telescope in Argentina and a DK 1.54 meter (Danish) telescope in Chile for the southern hemisphere open clusters. For the northern hemisphere, we observed in the Suhora observatory in Poland and the Adiyaman observatory in Turkey.

Our exposure time for each cluster is 300 seconds (5 minutes), and we do it twice for each cluster.

This work is just for Southern-Hemisphere clusters, which include 105 Galactic open clusters. Northern-hemisphere clusters are in the future plan.

We input the coordinates of the clusters into the Atlas of Large-Area Digital Image Navigation (Aladin), and then we see that it has a 270-degree rotation; we apply it to the clusters by writing a command in World Coordinate System (WCS) tools and rotate the RA and DEC of them. Then, we plot the X-Y with the magnitude scale of observed clusters, compare it with Aladin, and see the same structure in both.



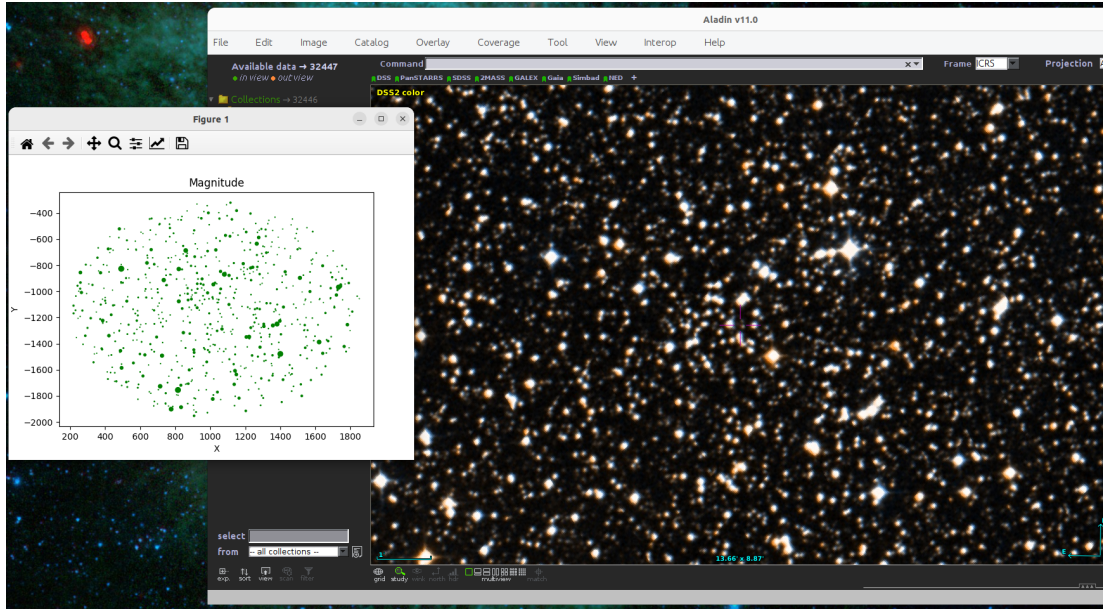


Figure 3.4: Comparing the X-Y with Magnitude scale with the sky for the cluster Teutsch 68

We reduce data in photometry via IRAF and get the Point Spread Function (PSF) and magnitude of all of them. Then we see that, in the images of the Casleo telescope, there are some cosmic rays. Then, in "imred," we use "Package = crutil" and "Task = cosmic rays" in IRAF to remove them and then get the new PSF without cosmic rays.

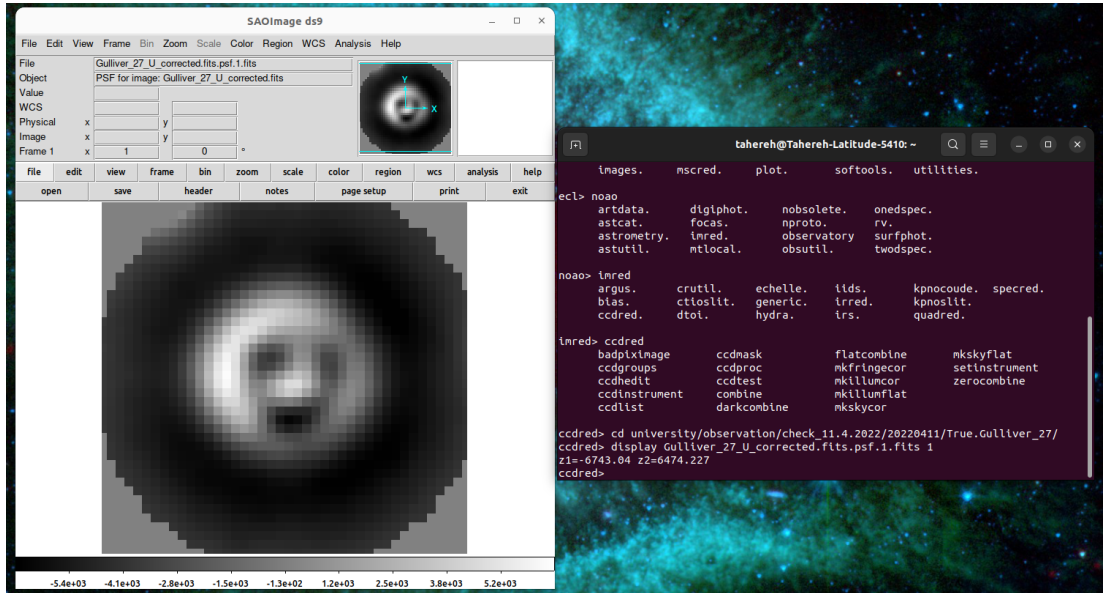


Figure 3.5: PSF of the DK 1.54 telescope

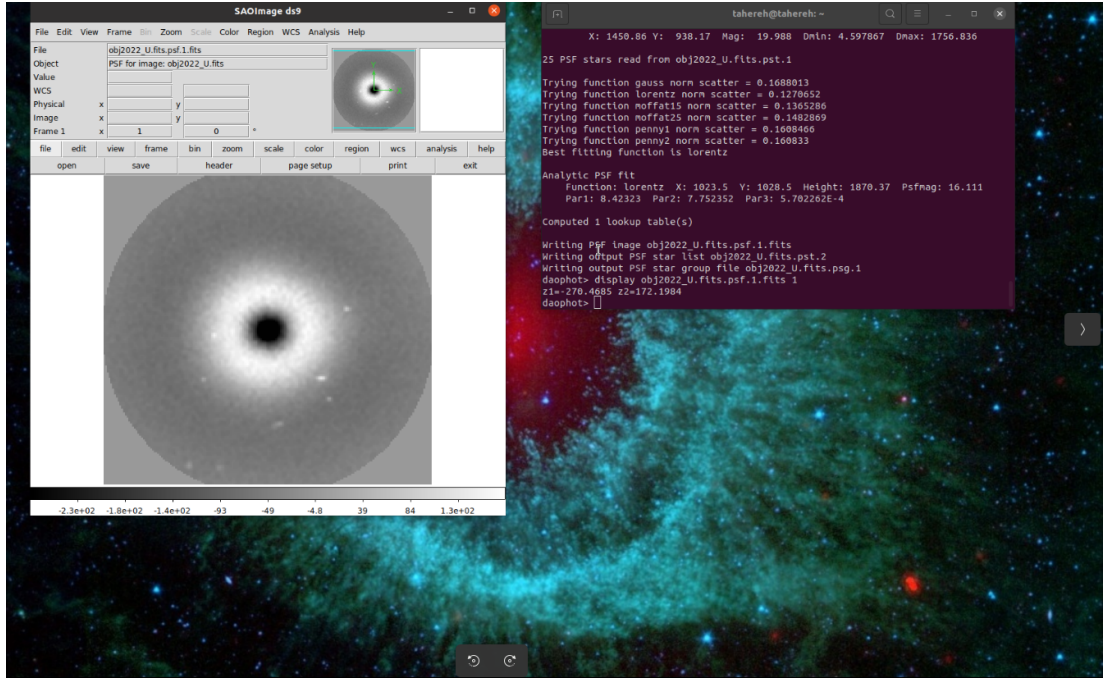


Figure 3.6: PSF with cosmic rays

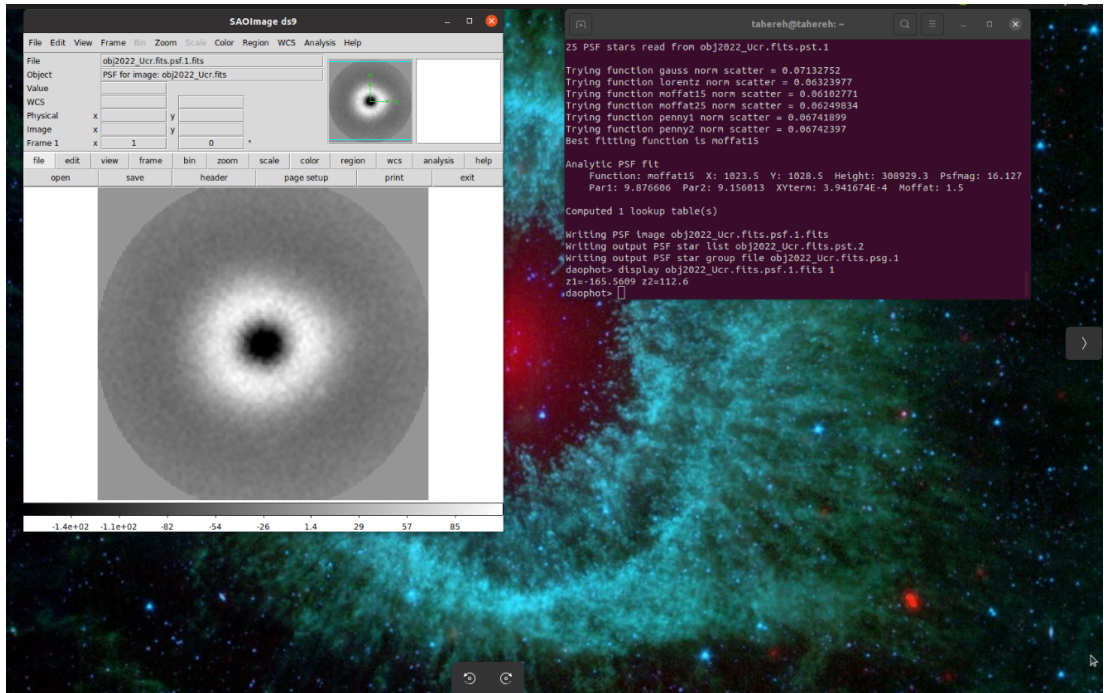


Figure 3.7: PSF without cosmic rays

Then, in IRAF, from the WCS, we use xy2sky to transform pixel coordinates (x, y) into the celestial coordinates (RA, DEC); afterwards, we can compare with an external catalogue like Gaia.

Then, from the Python code, we get all the stars of each cluster from Gaia DR3.

Instrumental magnitudes are typically raw values from the instrument (e.g., CCD), which depend on the specific setup (filters, detectors, exposure times). They are not directly comparable to the calibrated magnitudes from a survey like Gaia.

Gaia magnitudes are on an absolute, well-calibrated photometric system (e.g., G, BP, RP bands), while the instrumental magnitudes may have arbitrary zero points or scaling.

We use linear regression to ensure that our observed magnitudes can be directly compared to Gaia’s calibrated magnitudes, making our data scientifically accurate and meaningful.

We generate each cluster’s CSV file from RA, DEC, and Mag(U).

### 3.8.1 Matching The Observed Stars With Gaia DR3

After preparing the RA, DEC, and Mag(U) of the observations and getting the stars with their G, BP, and RP mag from the Gaia DR3, we match the observed stars with the Gaia DR3 epoch 2016.

To match stars from the Gaia and UV catalogues, we used a pipeline<sup>3</sup> based on the Match Program<sup>4</sup>, which uses the FOCAS algorithm (Valdes et al. 1995).

The script takes Gaia and UV tables in .CSV format as input data. Gaia data have been obtained for a given sky region using the script `get_stars_at_oc.py` available in the pipeline files.

It is also possible to load confirmed cluster members representing main sequence stars into the script. We used Hunt & Reffert (2023) catalogue based on Gaia DR3 data to define members.

We use the Match Program `project_coords` routine to convert RA and DEC coordinates into planar X and Y coordinates, using the coordinates of the object from the literature as the common centre.

The matching routine was used to match the stars from two catalogues. For this routine, we used the parameters:

`matchrad=3.0 trirad=0.001 nobj=40 recal`

The values of these parameters are explained in the Match Program manual<sup>5</sup>.

We then filtered the matched stars for cluster members.

Fitting is done manually, using a GUI interface that allows the main sequence isochrone to be shifted along two axes corresponding to the combination of colours selected. The script calculates the errors for a confidence interval of 99.73%.

A tutorial on the use of pipelines is available in the README.md file.

### 3.8.2 Our Comments For Hunt & Reffert Catalogue

Some of our observed clusters have another name in the Hunt & Reffert catalogue. We found their names in their catalogue and found the member’s probability.

---

<sup>3</sup><https://github.com/PoruchikRzhevsky/Match-pipeline>

<sup>4</sup><http://spiff.rit.edu/match/>

<sup>5</sup><http://spiff.rit.edu/match/match-0.16/match.html>

My comments to Hunt about their catalogue and her answers are as follows:

1) We see in your catalogue that one cluster (CWNU 1138) has two RA and DEC with different parameters' values:  $RA = 206.91188940$ ,  $DEC = -59.63303562$ , and  $RA = 196.27453631$ ,  $DEC = -59.71348582$ .

Answer: CWNU 1138 has tidal tails, which are standard in many nearby clusters.

2) When we put the Gaia ID of the members in part "Gaia DR3 source ID" of your catalogue, we see that for some clusters, their members belong to two or more clusters.

Answer: This is the case for some clusters, especially binary ones, that are difficult to separate from each other.

3) There were so many subclusters throughout the entire catalogue that the clusters did not survive; only their components remained.

Answer: Many regions have hierarchical star formation, and a given area can be split into many subclusters. It is a choice to divide things into more minor, which means we can catalogue all individual clusters. There could be times when not splitting clusters would be a better decision to take, but it can be challenging to know.

### 3.8.3 Colour-Colour Diagrams

We generate colour-colour diagrams from Colour-Magnitude Diagrams (CMDs), including U photometry and fit the filtered stars to find their extinction in each colour from the main sequence isochrone for the different colour combinations. The isochrone data are taken from the Padova isochrone (Bressan et al. 2012).

We get reddening from U in the colour-colour diagram, independent of age, distance, and metallicity. From a colour-colour diagram, we typically get reddened colours of stars. These observed colours include the effects of interstellar reddening, which is caused by dust and gas between the stars and the observer. We estimate the reddening for all our observed clusters in different passbands.

In the plots below, the red line is the main sequence isochrone. We shift the whole main sequence in x and y, we call the coefficients extinction in different filters like (U-G) and (BP-RP), and it shifts every point by the same magnitudes.

In the colour-colour diagrams, green dots are matched stars with Gaia DR3, in which in matched stars we have foreground and background stars or field stars, and pink triangles are members, which we obtained from Hunt & Reffert (2023) catalogue.

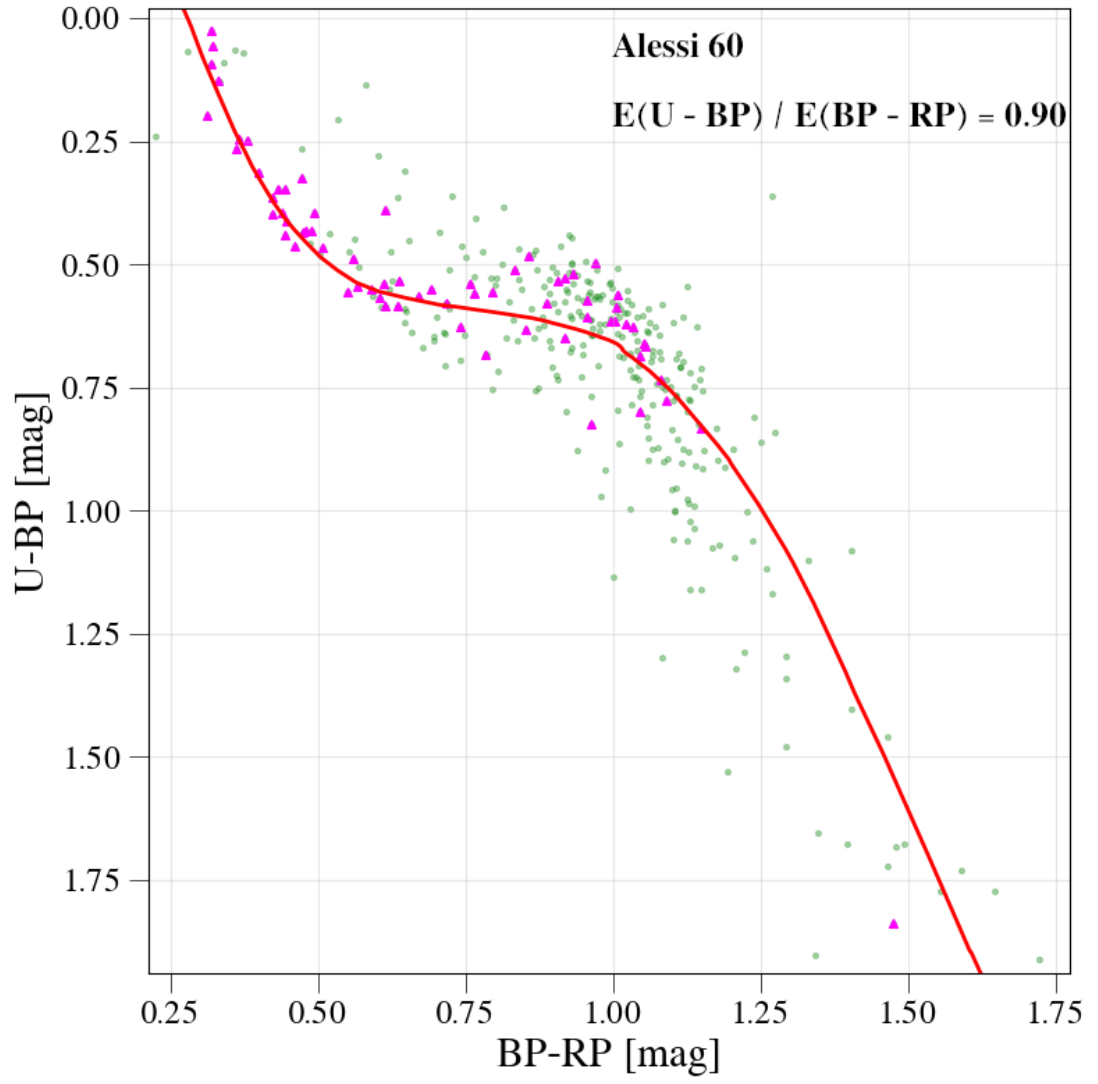


Figure 3.8: Colour–Colour Diagram of Alessi 60 in  $(U-BP)$  vs.  $(BP-RP)$ .

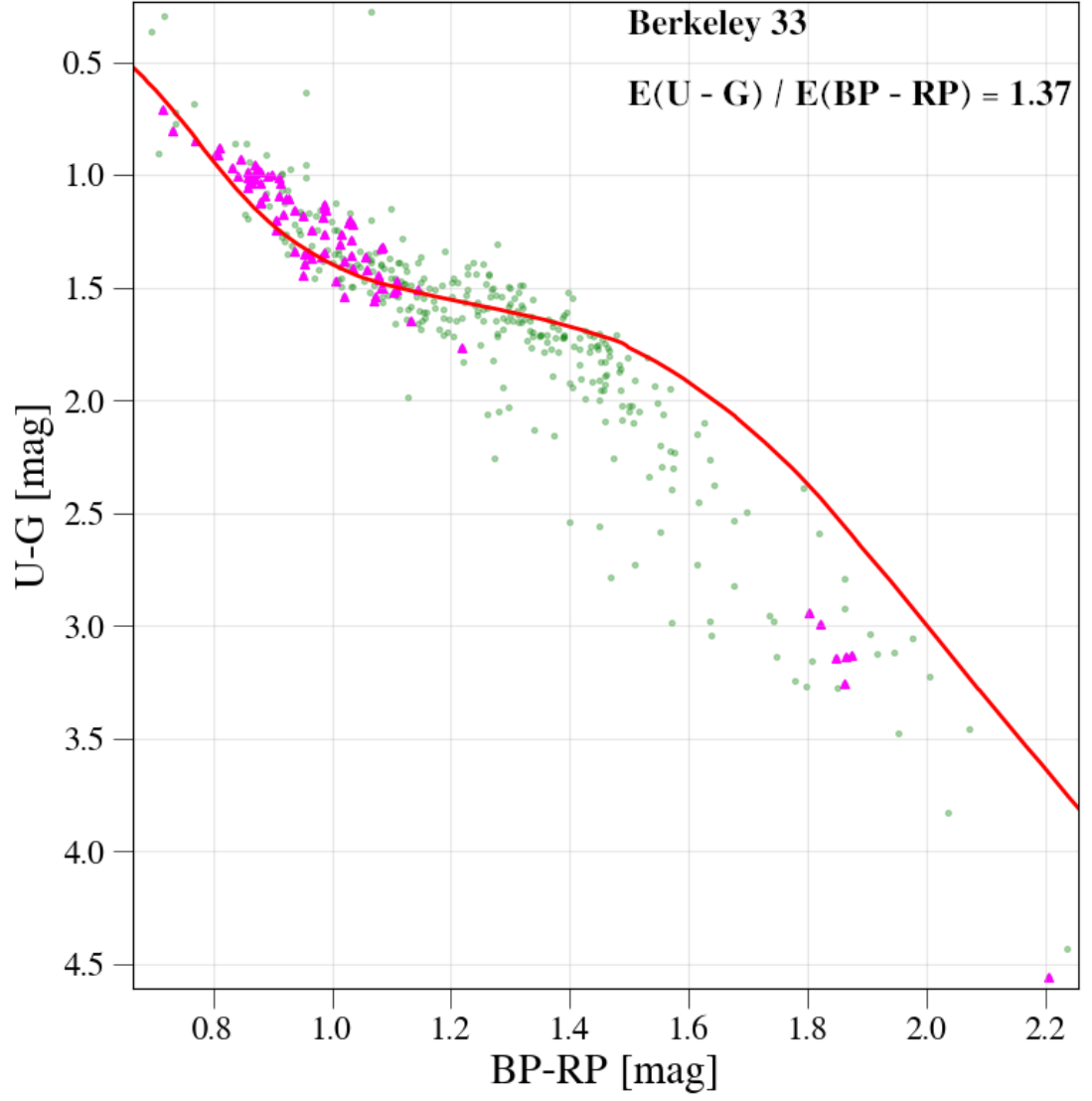


Figure 3.9: Colour–Colour Diagram of Berkeley 33 in  $(U-G)$  vs.  $(BP-RP)$ .

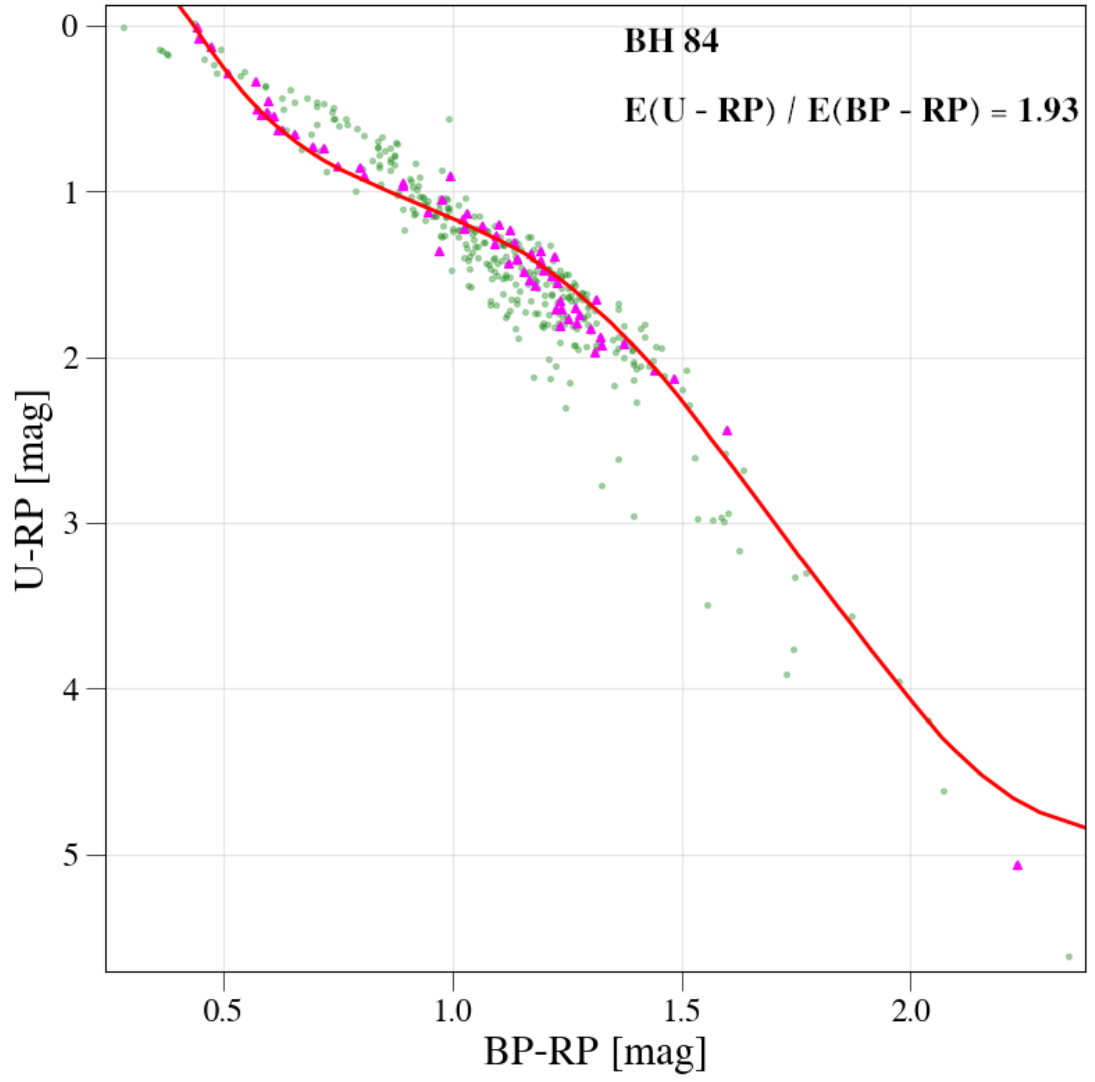


Figure 3.10: Colour–Colour Diagram of BH 84 in (U-RP) vs. (BP-RP).

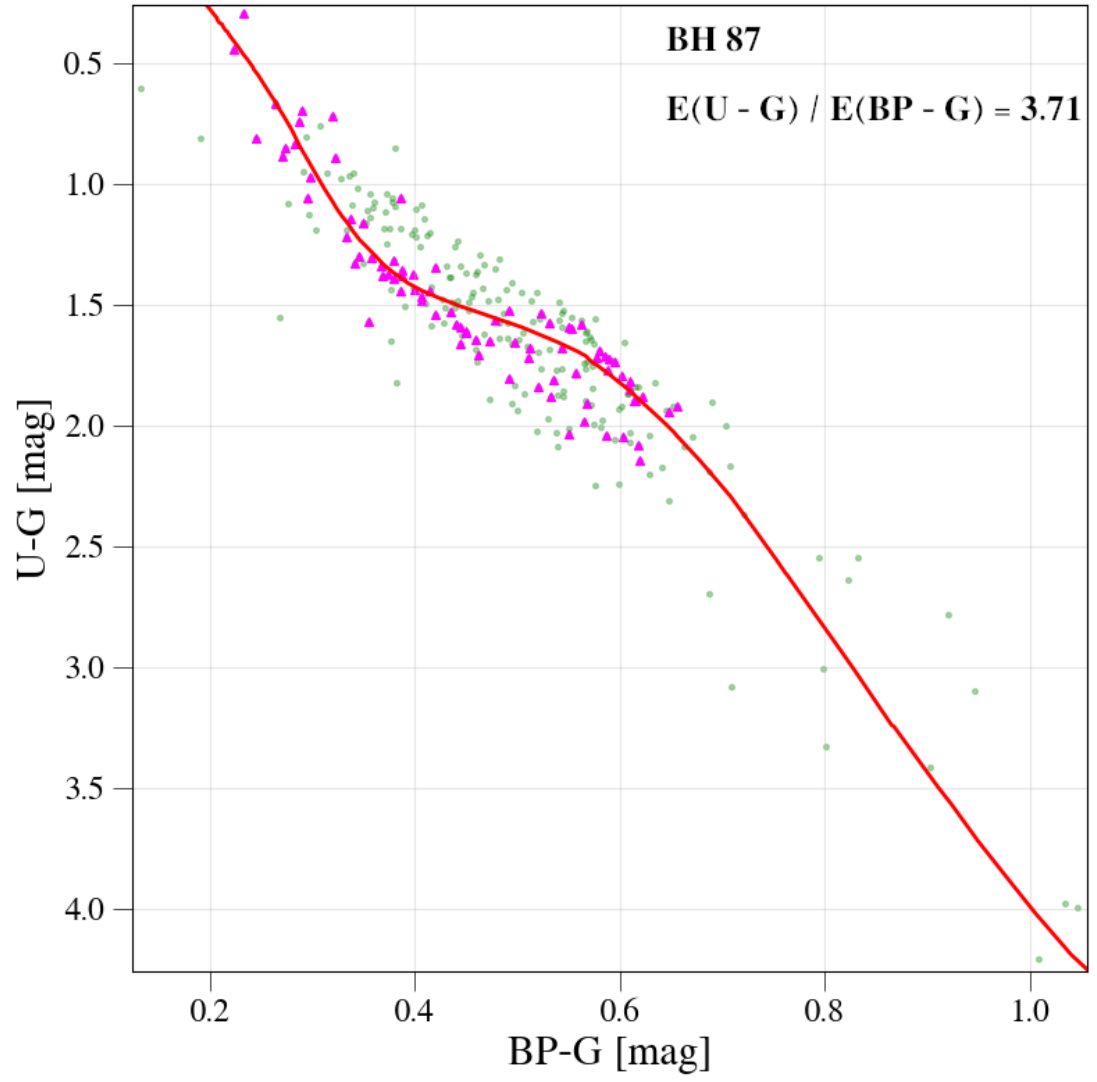


Figure 3.11: Colour–Colour Diagram of BH 87 in (U-G) vs. (BP-G).



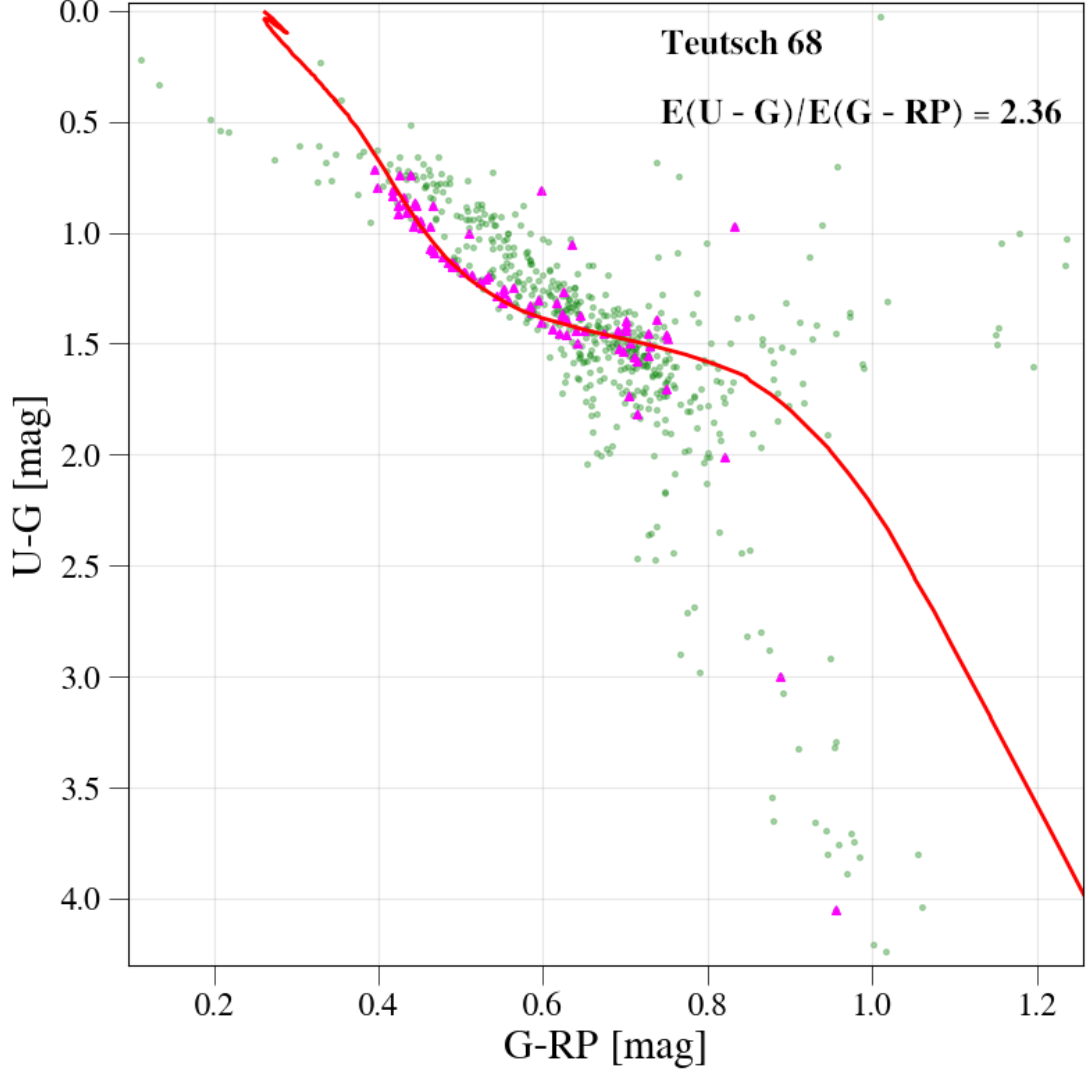


Figure 3.12: Colour–Colour Diagram of Teutsch 68 in (U-G) vs. (G-RP).

### 3.8.4 Reddening

Reddening occurs because of the scattering of light by dust and other matter present in the interstellar medium. The "colour excess" which is the difference between an object's intrinsic colour index (its standard colour index) and its observed colour index, is a measure of interstellar reddening. Stars appear redder than they are due to interstellar reddening, which happens when blue light waves are more heavily absorbed and scattered by interstellar dust than red light waves. This phenomenon is analogous to the effect of dust particles in Earth's atmosphere contributing to the reddish colours seen during sunset.

For example, the ratio  $E(U-G)/E(BP-RP)$  is an essential parameter. It indicates how interstellar dust affects different colour indices relative to each other. This ratio is crucial for characterizing the properties of the interstellar medium. We can describe the relative reddening effects on the (U-G) and (BP-RP) colour indices. This helps us understand how reddening influences the colours we observe in our data.

Central wavelengths are essential because the extinction varies with wavelength.

Below are the central wavelengths for the U, G, BP, and RP bands converted to angstroms ( $\text{\AA}$ ): (Bessell 2005), (Jordi et al. 2010)

- U Band (Ultraviolet) Central Wavelength:  $\sim 3650 \text{ \AA}$
- G Band (Gaia G) Central Wavelength:  $\sim 6730 \text{ \AA}$
- BP Band (Blue Photometer) Wavelength Range:  $3300\text{--}6800 \text{ \AA}$ ,  
Central Wavelength:  $\sim 5320 \text{ \AA}$
- RP Band (Red Photometer) Wavelength Range:  $6400\text{--}10500 \text{ \AA}$ ,  
Central Wavelength:  $\sim 7970 \text{ \AA}$

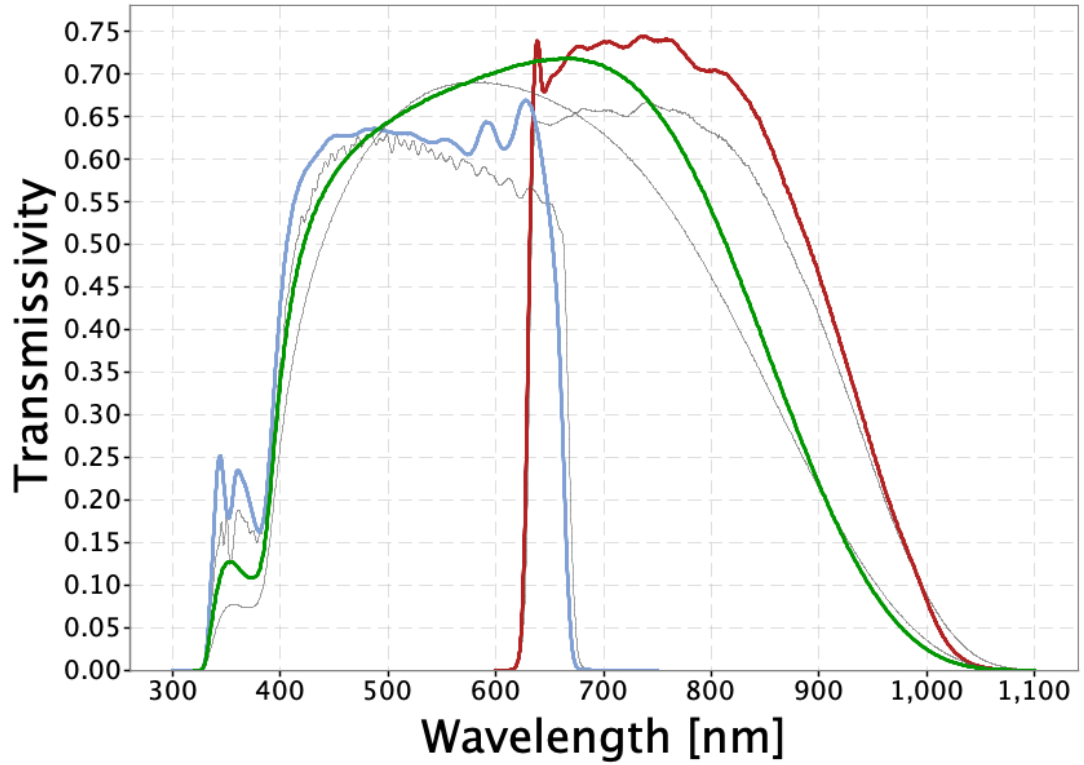


Figure 3.13: Central wavelengths for the U, G, BP, and RP bands.

Credits: ESA/Gaia/DPAC, P. Montegriffo, F. De Angeli, M. Bellazzini, E. Pancino, C. Cacciari, D. W. Evans, and CU5/PhotPipe team.

For two reasons, it is critical to understand the wavelength dependence of interstellar extinction, the light that interstellar dust grains absorb and scatter, and any spatial fluctuation in this dependence. The first is that the extinction depends on the optical characteristics of the dust grains along a line of sight, which can provide a visual view of the size distribution and composition of the grains.

Furthermore, the extent and kind of dust grain processing in the ISM may be revealed by variations in extinction from location to location. Second, as most

celestial objects are viewed through at least a tiny amount of interstellar dust, the wavelength dependence of extinction is necessary to eliminate the effects of dust obscuration from recorded energy distributions. Spatial differences in extinction may restrict how precisely energy distributions can be "dereddened." Such uncertainties may be tolerably minor for very weakly reddish objects, but along sight lines that are only slightly reddened, they can quickly become incapacitating (Fitzpatrick 1999).

### 3.9 Estimating The Clusters' Extinction

The precise interpretation or prediction of extinction, infrared emission, or reflection nebosity depends on the size distribution of interstellar dust particles. We must assess astrophysical processes like the photoelectric heating of interstellar gas and the creation of molecular hydrogen on grain surfaces. In addition, the size distribution is intriguing and closely related to the beginnings and development of grains (Kim et al. 1994).

Many processes can modify the grain size or composition distribution. Collisions between grains can lead to shattering, coagulation, or shattering and sticking together. In cold, dense regions, grains can accrete mantles of materials from the gas phase, which we will call "accretion." Deep within molecular clouds, icy mantles form in this way, perhaps starting with water and ammonia ices and continuing to frozen CO. Shocks can lead to sputtering of large grains and violent grain-grain collisions upon passage through the shock, or to evaporation of small grains because of their immersion in very hot shock-heated gas.

Although refractory components alone can only increase the overall volume of grains by 5%, the more significant depletion in dense regions indicates that there must be some growth of grains by accretion, which is why grains are more prominent in dense locations. Significant accretion growth requires components with high abundances (C, N, and O).

Accretion raises the grain volume and, thus, the overall extinction cross-section for each H nucleus. By allowing the constituent atoms to absorb collectively, slight grain expansion can increase the extinction per gram (Cardelli et al. 1989).

Using the ratios of two colors, such as  $E(U - B)/E(B - V)$ , to express the extinction law is not a novel approach in the literature. It is arbitrary to use  $A(V)$  as the visual's reference extinction (Cardelli et al. 1989).

The outcomes of our extinction estimation in  $[X, Y]$  coordinates are shown in Figures 14 and 15. The Y coordinate shows the disk rotation, whereas the X coordinate indicates the Galactic center. The Sun is in that order at  $[0, 0]$ . Our research does not consider the third coordinate  $[Z]$  because every star cluster under study is found in the Galactic disk.

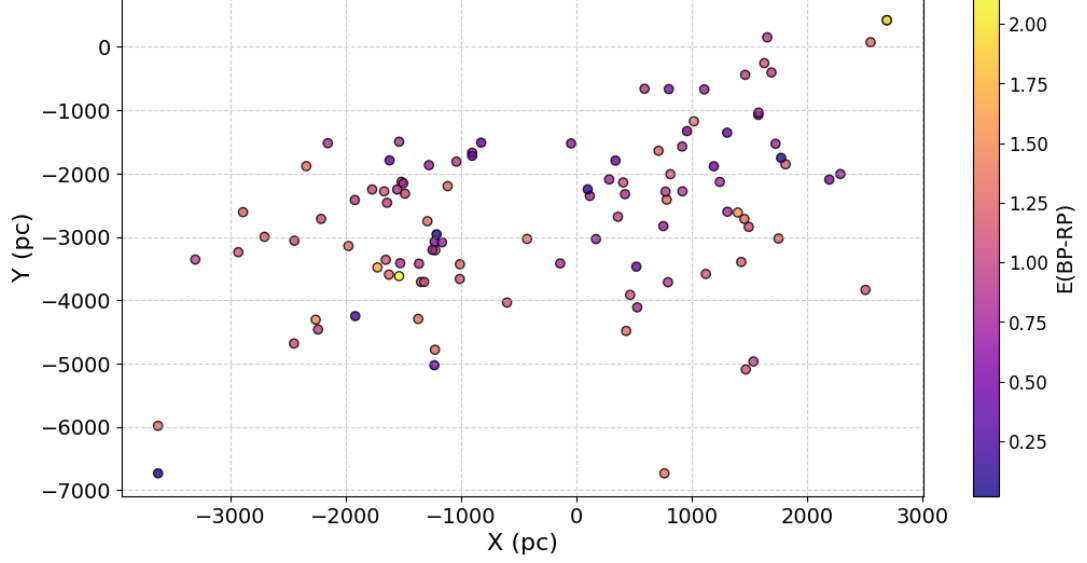


Figure 3.14: Extinction in  $(\text{BP} - \text{RP})$  for the 105 observed clusters in the  $[X, Y]$  coordinate system around the Sun at  $[0, 0]$ .

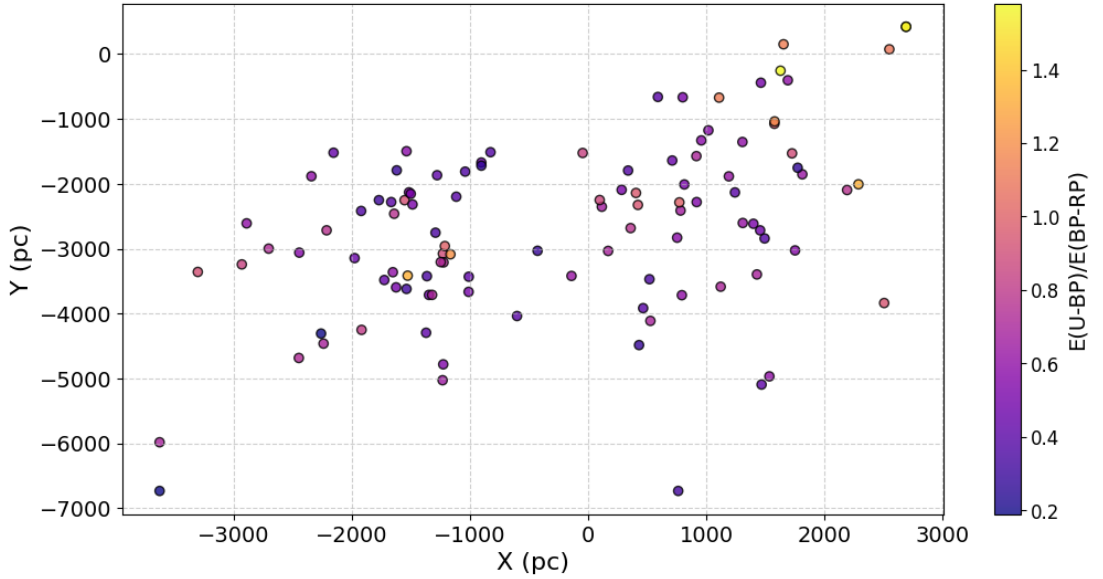


Figure 3.15: Reddening ratio  $E(\text{U} - \text{BP})/E(\text{BP} - \text{RP})$  for the 105 observed clusters in the  $[X, Y]$  coordinate system around the Sun at  $[0, 0]$ .

For increasingly distant clusters, the extinction is growing with few exceptions (Figure 15). The present models predict this, which gives our fitting process more confidence. Exciting aspects may be seen in the reddening ratio distribution (Fig. 2, lower panel). For instance, there are some abrupt changes on small scales  $[-1000, -3000]$ , a continuous transition in the direction  $[-3000, -3000]$ , and no changes in some lines of sight. It demonstrates the capacity to track the ISM using star cluster extinction estimates.

In the below tables, from left to right, we represent the names of the clusters, their coordinates in RA and DEC, different extinction ratios, uncertainties of each extinction's ratios, and the mean value of extinctions. Also we get the distance in kilo parsec and log age in year from Hunt & Reffert (2023) catalogue. Just the cluster BH 140 doesn't have log age in their catalogue.

Table 3.1: Coordinates, reddening values, and uncertainties of clusters. The columns denote: (1) Clusters' name. (2) Right ascension (J2000; Gaia DR3). (3) Declination (J2000; GaiaDR3). (4) E(U-BP)/E(BP-RP). (5) E(U-G)/E(BP-RP). (6) E(U-RP)/E(BP-RP). (7) E(U-G)/E(G-RP). (8) E(U-G)/E(BP-G). (9) Uncertainty of E(U-BP)/E(BP-RP). (10) Uncertainty of E(U-G)/E(BP-RP). (11) Uncertainty of E(U-RP)/E(BP-RP). (12) Uncertainty of E(U-G)/E(G-RP). (13) Uncertainty of E(U-G)/E(BP-G). (14) Mean extinction. (15) Distance (50) (kpc). (16) LogAge (50) (yr).

(1)	(2)	(3)	(4)	(5)	(6)	(7)	(8)	(9)	(10)	(11)	(12)	(13)	(14)	(15)	(16)
Alessi_17	113.853	-15.092	1.08	1.36	2.01	2.08	3.78	0.28	0.11	0.17	0.76	0.41	2.06	3.92	8.38
Alessi_60	105.615	-1.120	0.90	1.29	1.90	2.03	2.09	0.14	0.09	0.08	0.22	0.20	1.64	2.64	8.68
Berkeley_33	104.454	-13.226	0.98	1.37	1.98	2.24	3.45	0.08	0.10	0.08	0.29	0.16	2.00	4.73	8.68
BH_72	142.843	-53.041	1.30	1.68	2.30	2.18	2.98	0.55	0.56	0.57	0.80	0.88	2.09	4.51	8.23
BH_84	150.334	-58.217	0.92	1.33	1.93	2.21	3.22	0.12	0.13	0.13	0.34	0.35	1.92	3.80	8.21
BH_87	151.162	-55.377	1.13	1.54	2.13	2.52	3.71	0.11	0.10	0.08	0.21	0.27	2.21	2.18	8.15
BH_111	167.317	-63.830	0.91	1.30	1.91	2.15	3.32	0.23	0.24	0.22	0.51	0.53	1.92	2.46	8.43
BH_132	186.725	-64.065	0.85	1.32	1.85	1.93	3.45	0.31	0.32	0.32	0.46	0.32	1.88	2.47	7.98
BH_140	193.454	-67.182	1.16	1.55	2.17	2.84	3.44	0.06	0.07	0.07	0.38	0.39	2.23	4.60	
CWNU_95	223.299	-54.108	0.59	1.00	1.63	1.63	2.60	0.18	0.17	0.18	0.68	0.74	1.49	1.05	7.37
CWNU_1733	114.240	-26.321	0.39	0.89	1.45	1.51	2.11	0.27	0.32	0.28	0.71	0.80	1.27	1.73	8.30
Czernik_29	112.095	-15.399	1.08	1.41	2.08	2.44	3.66	0.09	0.10	0.07	0.32	0.21	2.13	3.51	8.39
Czernik_31	114.241	-20.522	0.97	1.42	1.97	2.28	2.96	0.11	0.11	0.10	0.13	0.38	1.92	2.96	8.19
Czernik_32	117.617	-29.853	0.88	1.30	1.82	2.22	2.73	0.10	0.13	0.12	0.43	0.19	1.79	3.74	8.86
ESO_368-14	116.751	-32.963	0.62	1.13	1.64	1.65	1.67	0.36	0.26	0.24	0.88	0.78	1.35	3.32	7.99
ESO_559-13	112.178	-20.802	0.72	1.15	1.77	1.79	2.64	0.28	0.25	0.27	0.51	0.57	1.61	2.26	8.82
FSR_1183	108.354	-9.891	0.88	1.33	1.88	2.31	3.05	0.17	0.15	0.17	0.31	0.79	1.89	2.15	8.49
FSR_1260	112.090	-19.684	1.34	1.71	2.27	2.52	4.41	0.28	0.25	0.22	0.44	0.58	2.45	2.62	8.14
FSR_1352	116.613	-34.295	0.74	1.13	1.69	1.96	2.65	0.14	0.12	0.10	0.22	0.28	1.63	3.31	6.92
FSR_1402	136.433	-37.878	1.13	1.63	2.13	2.86	2.96	0.13	0.13	0.09	0.23	0.20	2.14	4.11	9.10
FSR_1407	142.455	-33.851	1.32	1.63	2.32	2.39	2.85	0.32	0.24	0.24	0.58	0.41	2.10	3.14	9.43
FSR_1703	235.392	-54.971	0.64	1.18	1.64	2.23	2.31	0.08	0.09	0.09	0.49	0.23	1.60	1.91	7.97
Gulliver_7	141.751	-55.126	1.36	1.82	2.46	3.27	3.45	0.63	0.41	0.38	0.81	0.32	2.47	6.79	8.29
Gulliver_39	163.696	-58.051	1.32	1.80	2.32	3.05	4.25	0.23	0.16	0.18	0.58	0.91	2.55	2.54	8.72
Gulliver_58	191.504	-61.972	0.53	1.21	1.71	1.73	2.06	0.30	0.35	0.41	0.36	0.55	1.45	2.23	8.13
Haffner_4	106.515	-15.005	1.17	1.57	2.17	2.53	3.94	0.14	0.13	0.12	0.41	0.35	2.27	4.05	8.71
Haffner_6	109.998	-13.153	1.15	1.55	2.16	2.68	3.81	0.13	0.12	0.10	0.26	0.25	2.27	4.37	8.64
Haffner_9	111.180	-16.997	1.15	1.55	2.16	2.68	3.81	0.13	0.12	0.10	0.26	0.25	2.12	2.86	8.31
Haffner_11	113.841	-27.714	1.07	1.44	2.03	3.39	3.84	0.15	0.52	0.37	0.87	0.79	2.35	5.30	8.76
Haffner_17	117.898	-31.815	0.02	0.46	1.02	1.05	1.10	0.12	0.16	0.13	0.58	0.68	0.73	3.20	7.96
Haffner_20	119.063	-30.369	2.11	2.47	2.95	4.03	4.06	0.53	0.46	0.36	0.83	0.92	3.12	3.93	8.31
Haffner_21	120.290	-27.219	1.30	1.70	2.30	2.83	4.80	0.27	0.17	0.16	0.31	0.83	2.59	3.04	8.48
HSC_71	270.242	-24.870	0.92	1.31	1.90	2.51	3.05	0.39	0.41	0.43	0.87	0.94	1.94	1.66	7.53
HSC_2281	149.274	-56.046	0.84	1.32	1.85	2.19	3.02	0.09	0.09	0.08	0.29	0.23	1.84	2.36	8.06
LP_1182	238.110	-55.418	0.82	1.27	1.85	2.28	2.87	0.25	0.28	0.28	0.80	0.53	1.82	1.89	8.00
Melotte_72	114.619	-10.701	0.40	1.02	1.67	1.70	2.46	0.13	0.15	0.15	0.35	0.26	1.45	2.43	9.11
NGC_2225	96.646	-9.644	1.32	1.77	2.47	3.64	3.98	0.21	0.19	0.10	0.60	0.27	2.64	3.05	9.16
NGC_2425	114.572	-14.884	0.94	1.40	1.94	2.60	2.94	0.10	0.09	0.10	0.38	0.25	1.97	3.09	9.30
NGC_2588	125.799	-32.968	1.34	1.74	2.34	2.76	4.53	0.33	0.18	0.18	0.37	0.85	2.54	4.51	8.69
NGC_2635	129.625	-34.778	1.27	1.57	2.27	2.51	4.57	0.14	0.13	0.11	0.29	0.29	2.44	4.95	8.65
NGC_2658	130.865	-32.662	1.11	1.53	2.11	2.41	3.92	0.10	0.07	0.06	0.12	0.23	2.22	3.82	8.65
NGC_3255	156.633	-60.676	1.11	1.42	1.96	2.20	3.74	0.15	0.14	0.13	0.30	0.42	2.09	5.31	8.42
NGC_6334	259.952	-36.083	1.12	1.69	2.14	3.10	3.13	0.32	0.25	0.24	0.74	0.90	2.24	1.65	7.09

Table 3.2: Continuous in Table 3.1.

(1)	(2)	(3)	(4)	(5)	(6)	(7)	(8)	(9)	(10)	(11)	(12)	(13)	(14)	(15)	(16)
OC_0015	271.268	-21.206	1.09	1.51	2.10	2.80	3.42	0.20	0.19	0.20	0.35	0.40	2.19	2.73	7.25
OC_0501	137.252	-46.433	0.67	1.14	1.73	2.28	2.49	0.32	0.42	0.34	0.99	0.51	1.66	1.53	7.71
OC_0510	140.340	-50.772	0.82	1.25	1.80	2.47	3.40	0.52	0.56	0.57	0.86	0.97	1.95	2.36	8.06
OC_0523	144.667	-54.508	0.83	1.38	1.92	2.27	3.20	0.16	0.45	0.31	0.51	0.90	1.92	4.15	7.87
OC_0531	147.063	-58.177	0.45	0.90	1.50	1.53	2.24	0.17	0.17	0.20	0.52	0.64	1.33	1.83	8.22
OC_0596	198.856	-61.592	0.56	1.10	1.68	1.99	2.05	0.80	0.88	0.84	0.64	0.88	1.48	1.64	8.51
OC_0621	225.895	-60.003	0.75	1.30	1.72	2.53	2.59	0.16	0.16	0.20	0.71	0.33	1.78	3.05	7.80
OC_0673	252.621	-41.595	0.94	1.28	1.94	2.09	3.01	0.33	0.25	0.34	0.75	0.93	1.85	1.53	6.86
OC_0677	255.064	-38.784	0.96	1.37	1.96	2.19	2.68	0.43	0.42	0.46	0.96	0.89	1.83	1.74	8.27
PHOC_27	135.960	-53.849	0.75	1.20	1.75	2.01	2.90	0.10	0.09	0.08	0.22	0.31	1.72	3.05	8.18
Pismis_15	143.684	-48.046	0.15	0.66	1.23	1.35	1.50	0.08	0.09	0.08	0.21	0.16	0.98	2.25	8.65
Ruprecht_4	102.245	-10.530	1.22	1.71	2.22	2.57	3.81	0.14	0.13	0.10	0.35	0.22	2.31	3.91	8.76
Ruprecht_16	110.794	-19.499	1.16	1.46	2.18	3.07	4.02	0.26	0.19	0.17	0.64	0.63	2.38	2.83	8.39
Ruprecht_25	114.198	-23.386	1.30	1.84	2.32	3.74	4.15	0.59	0.40	0.43	0.92	0.66	2.67	7.00	8.64
Ruprecht_27	114.417	-26.513	0.77	1.16	1.77	1.95	2.83	0.09	0.08	0.07	0.31	0.26	1.70	1.90	8.60
Ruprecht_28	114.904	-30.935	1.27	1.77	2.39	2.81	3.94	0.15	0.13	0.11	0.30	0.22	2.44	3.96	9.08
Ruprecht_29	115.244	-24.398	0.93	1.44	2.07	2.20	3.70	0.33	0.32	0.31	0.49	0.95	2.07	2.09	7.98
Ruprecht_41	118.424	-27.007	1.13	1.48	2.14	2.56	3.93	0.16	0.14	0.14	0.38	0.27	2.25	3.75	8.46
Ruprecht_42	119.404	-25.925	0.96	1.27	2.02	2.25	3.49	0.11	0.09	0.10	0.25	0.30	2.00	5.00	8.75
Ruprecht_44	119.692	-28.547	0.23	0.59	1.10	1.11	1.91	0.19	0.19	0.26	0.34	0.57	0.99	4.66	7.31
Ruprecht_48	120.681	-32.046	1.55	1.95	2.52	3.22	5.35	0.16	0.15	0.12	0.24	0.95	2.92	3.44	8.04
Ruprecht_54	122.850	-31.942	1.26	1.61	2.26	2.88	3.88	0.24	0.21	0.23	0.59	0.43	2.38	3.95	8.90
Ruprecht_75	140.487	-56.317	1.13	1.66	2.13	2.87	3.49	0.21	0.18	0.22	0.43	0.37	2.26	3.96	8.90
Ruprecht_82	146.416	-54.003	0.81	1.20	1.81	2.01	2.95	0.11	0.10	0.10	0.37	0.29	1.76	2.11	8.65
Ruprecht_83	147.310	-54.609	0.48	1.23	1.68	1.73	2.99	0.26	0.48	0.35	0.42	0.81	1.62	3.51	8.01
Ruprecht_100	181.507	-62.628	1.06	1.40	2.06	3.02	4.20	0.27	0.31	0.28	0.50	0.61	2.35	3.21	8.37
Ruprecht_101	182.410	-62.990	1.31	1.74	2.14	3.18	3.78	0.32	0.31	0.21	0.46	0.70	2.43	3.08	8.76
SAI_86	122.053	-36.609	1.23	1.77	2.23	2.88	3.36	0.28	0.24	0.30	0.91	0.99	2.29	3.58	8.55
SAI_91	129.234	-50.045	0.84	1.27	1.83	2.19	2.97	0.11	0.08	0.08	0.18	0.34	1.82	3.44	8.55
Teutsch_61	113.663	-19.787	0.86	1.32	1.86	2.27	3.21	0.10	0.09	0.08	0.20	0.36	1.91	2.74	7.55
Teutsch_68	146.080	-54.115	1.02	1.38	1.99	2.36	3.49	0.09	0.09	0.08	0.25	0.21	2.05	2.71	8.42
Teutsch_210	114.531	-21.555	1.01	1.34	2.01	2.29	3.66	0.19	0.15	0.11	0.26	0.44	2.06	2.75	8.37
Teutsch_J1037.3-6034	159.517	-60.516	0.98	1.37	1.98	2.11	3.84	0.19	0.19	0.17	0.51	0.71	2.06	5.20	8.50
Theia_2115	239.415	-53.064	0.77	1.29	1.77	2.48	2.57	0.11	0.16	0.12	0.40	0.31	1.78	1.30	7.57
Theia_5150	121.532	-33.102	1.09	1.47	2.08	2.58	3.95	0.14	0.13	0.12	0.27	0.21	2.23	3.94	8.32
Theia_5496	211.390	-64.155	1.34	1.73	2.37	2.94	4.43	0.33	0.25	0.21	0.79	0.99	2.56	1.56	8.70
Trumpler_9	118.915	-25.883	1.28	1.66	2.28	2.88	4.32	0.35	0.29	0.23	0.59	0.81	2.48	2.47	8.00
Trumpler_17	164.103	-59.227	0.94	1.33	1.94	2.24	3.22	0.07	0.07	0.09	0.17	0.16	1.93	2.41	7.72
UBC_261	159.952	-60.469	1.17	1.52	2.17	2.41	4.00	0.12	0.13	0.12	0.33	0.42	2.26	3.76	7.96
UBC_273	170.317	-60.565	1.18	1.54	2.18	2.51	4.15	0.24	0.24	0.22	0.40	0.77	2.31	2.17	7.70
UBC_275	167.716	-65.713	1.20	1.54	2.21	2.56	4.13	0.20	0.23	0.20	0.69	0.24	2.33	3.70	8.52
UBC_277	173.989	-59.490	1.22	1.61	2.16	2.46	4.06	0.68	0.70	0.72	0.75	0.66	2.30	1.79	8.01
UBC_282	180.157	-60.484	0.83	1.20	1.83	1.96	2.97	0.12	0.14	0.13	0.36	0.20	1.75	2.92	8.17
UBC_296	216.171	-61.056	0.47	0.84	1.41	1.53	2.22	0.10	0.09	0.10	0.20	0.22	1.30	1.88	8.02

Table 3.3: Continuous in Table 3.1.

(1)	(2)	(3)	(4)	(5)	(6)	(7)	(8)	(9)	(10)	(11)	(12)	(13)	(14)	(15)	(16)
UBC_297	218.062	-62.212	1.23	1.86	2.42	2.83	3.94	0.36	0.34	0.18	0.70	0.51	2.46	2.59	8.23
UBC_336	267.982	-27.851	1.25	1.82	2.28	3.18	4.08	0.13	0.12	0.12	0.41	0.22	2.52	2.55	8.14
UBC_457	109.845	-21.418	0.76	1.31	1.76	1.89	3.25	0.14	0.17	0.10	0.21	0.39	1.79	2.63	8.18
UBC_463	116.557	-26.206	0.43	0.84	1.50	1.50	2.21	0.23	0.21	0.22	0.33	0.76	1.30	1.94	8.10
UBC_498	155.133	-59.700	0.74	1.13	1.74	1.76	2.94	0.18	0.19	0.19	0.47	0.51	1.66	2.93	8.01
UBC_516	182.517	-62.330	1.57	2.01	2.55	2.85	4.77	0.28	0.21	0.17	0.74	0.84	2.75	2.97	8.48
UBC_520	186.112	-66.672	0.83	1.21	1.83	2.10	3.00	0.12	0.12	0.10	0.31	0.29	1.79	1.82	8.63
UBC_637	123.758	-22.211	1.48	1.90	2.48	2.85	3.60	0.44	0.37	0.34	0.82	0.84	2.46	4.90	9.33
UBC_1385	116.746	-20.973	1.27	1.72	2.27	2.80	3.81	0.24	0.17	0.13	0.34	0.51	2.37	3.72	8.64
UBC_1396	118.502	-26.760	1.71	2.00	2.57	3.10	5.06	0.68	0.41	0.34	0.56	0.96	2.89	3.89	8.19
UBC_1417	121.268	-30.697	0.91	1.42	2.02	2.62	3.65	0.38	0.30	0.29	0.52	0.87	2.12	3.69	8.56
UBC_1420	119.585	-32.152	0.67	1.04	1.63	2.18	2.60	0.17	0.18	0.15	0.93	0.30	1.62	3.44	8.40
UBC_1515	186.704	-62.380	1.25	1.70	2.22	3.00	3.15	0.46	0.48	0.48	0.93	0.97	2.26	3.50	8.47
UBC_1528	217.652	-59.115	0.08	0.75	1.16	1.39	1.54	0.63	0.72	0.70	0.49	0.73	0.99	2.49	8.65
UBC_1529	221.430	-61.070	0.62	1.15	1.70	2.22	2.41	0.15	0.13	0.13	0.43	0.57	1.62	3.03	7.95
UBC_1534	222.947	-57.739	0.76	1.26	1.77	2.48	2.52	0.27	0.44	0.32	0.65	0.61	1.76	2.31	8.03
UBC_1592	213.573	-64.190	0.91	1.33	1.91	2.12	3.29	0.15	0.18	0.16	0.47	0.40	1.91	0.89	7.75
UFMG_58	124.879	-38.272	0.44	0.92	1.49	1.67	1.71	0.72	0.88	0.89	0.80	0.43	1.24	5.18	8.35



In the following, we show the scatter plots of extinctions vs. their uncertainties. We see that there is no correlation between extinctions and their uncertainties.

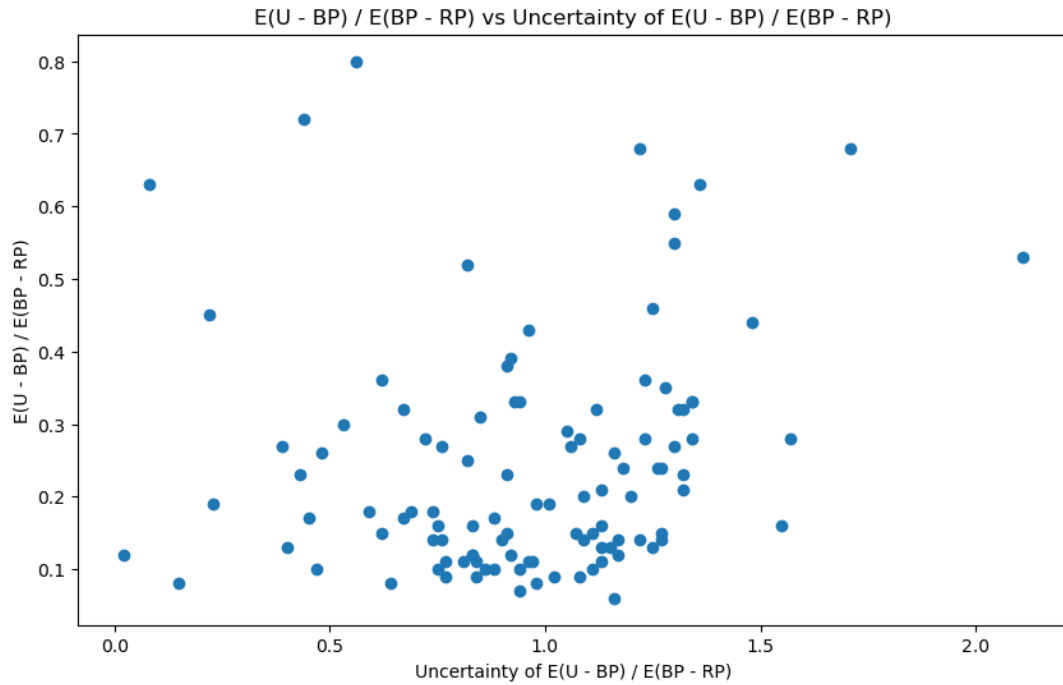


Figure 3.16: Correlation of  $E(U - BP)/E(BP - RP)$  vs. Uncertainty of  $E(U - BP)/E(BP - RP)$

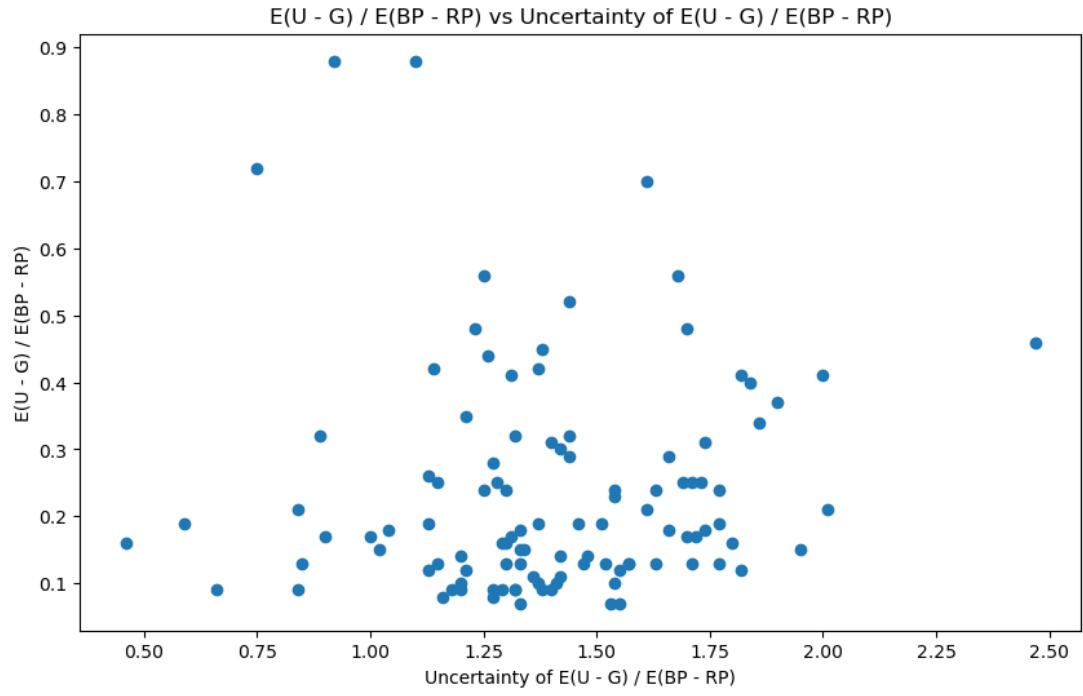


Figure 3.17: Correlation of  $E(U - G)/E(BP - RP)$  vs. Uncertainty of  $E(U - G)/E(BP - RP)$

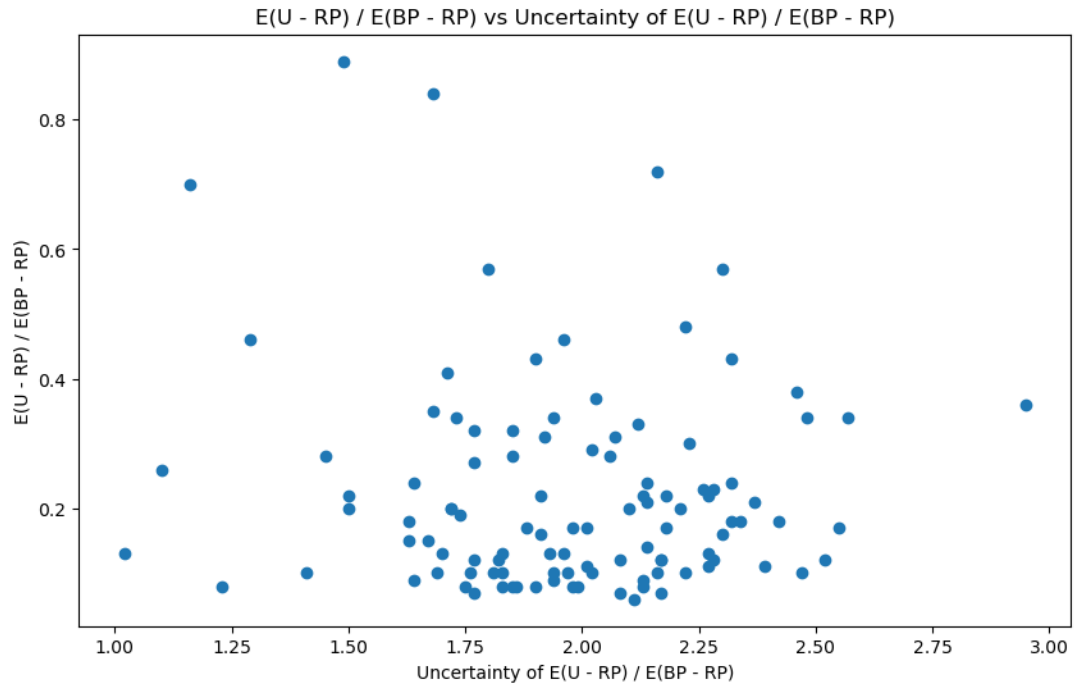


Figure 3.18: Correlation of  $E(U - RP)/E(BP - RP)$  vs. Uncertainty of  $E(U - RP)/E(BP - RP)$

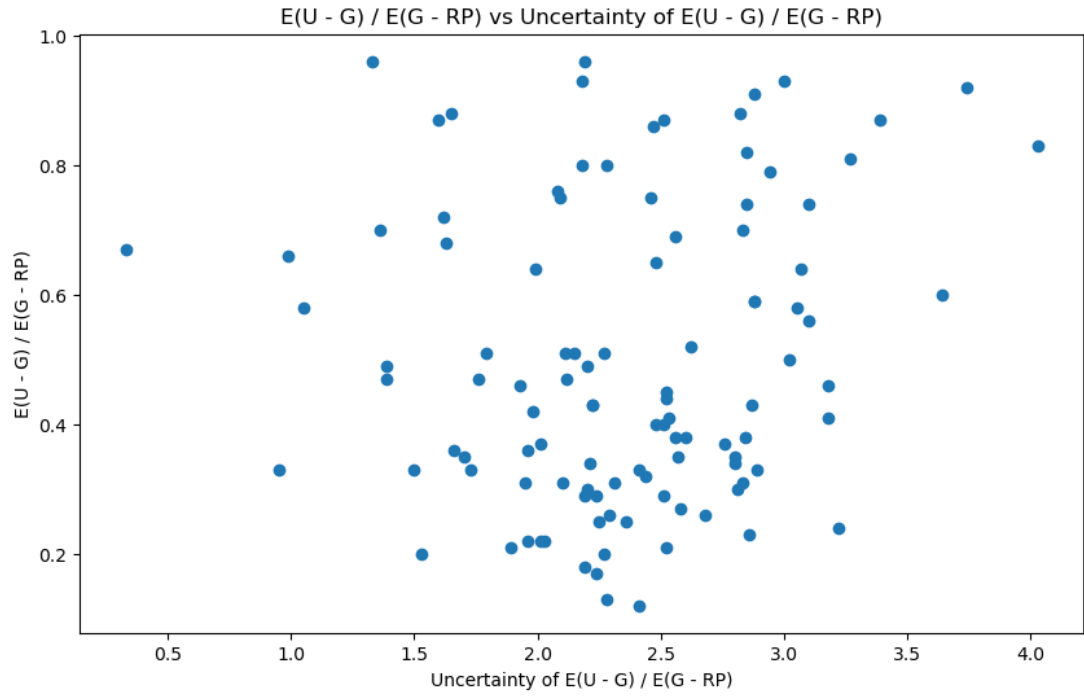


Figure 3.19: Correlation of  $E(U - G)/E(G - RP)$  vs. Uncertainty of  $E(U - G)/E(G - RP)$

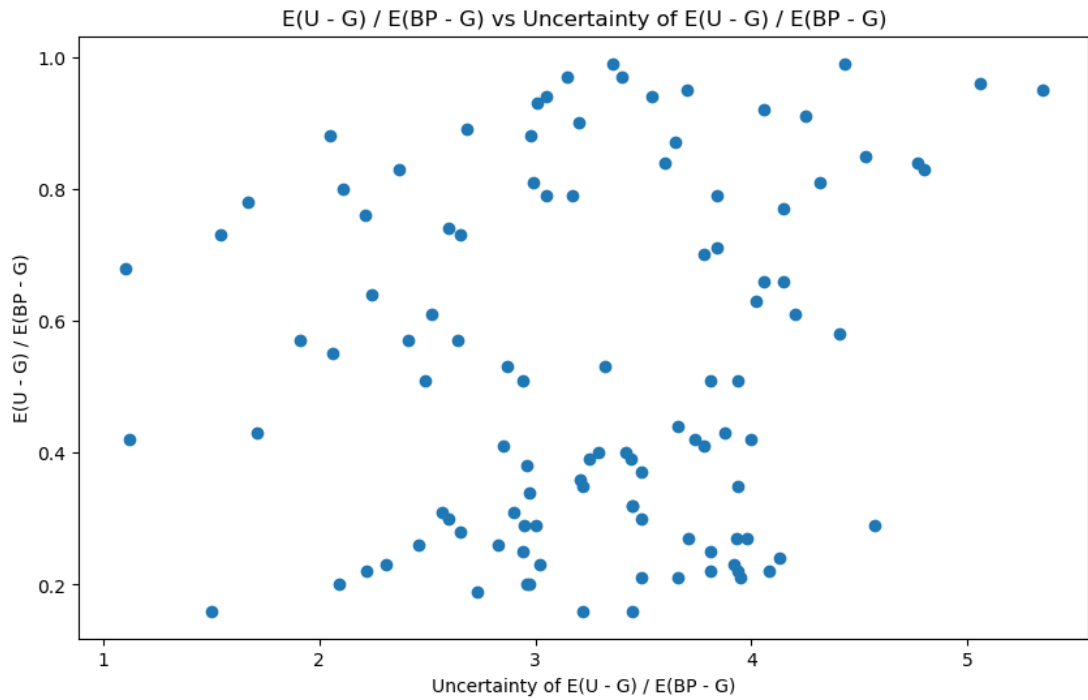


Figure 3.20: Correlation of  $E(U - G)/E(BP - G)$  vs. Uncertainty of  $E(U - G)/E(BP - G)$

We get Uncertainties from these formulas (Lee & Forthofer 2006):

$$\frac{E(U - BP)}{E(BP - RP)} \times \sqrt{\left(\frac{\sigma_{E(U-BP)}}{E(U - BP)}\right)^2 + \left(\frac{\sigma_{E(BP-RP)}}{E(BP - RP)}\right)^2}$$

$$\frac{E(U - G)}{E(BP - RP)} \times \sqrt{\left(\frac{\sigma_{E(U-G)}}{E(U - G)}\right)^2 + \left(\frac{\sigma_{E(BP-RP)}}{E(BP - RP)}\right)^2}$$

$$\frac{E(U - RP)}{E(BP - RP)} \times \sqrt{\left(\frac{\sigma_{E(U-RP)}}{E(U - RP)}\right)^2 + \left(\frac{\sigma_{E(BP-RP)}}{E(BP - RP)}\right)^2}$$

$$\frac{E(U - G)}{E(G - RP)} \times \sqrt{\left(\frac{\sigma_{E(U-G)}}{E(U - G)}\right)^2 + \left(\frac{\sigma_{E(G-RP)}}{E(G - RP)}\right)^2}$$

$$\frac{E(U - G)}{E(BP - G)} \times \sqrt{\left(\frac{\sigma_{E(U-G)}}{E(U - G)}\right)^2 + \left(\frac{\sigma_{E(BP-G)}}{E(BP - G)}\right)^2}$$

In the above formulas, sigma is the uncertainty.

We have not found any resources with which to compare our results.

In the plot below, we define the positions of all clusters in the Milky Way. The colour and size of each point are proportional to the mean extinction of the cluster.

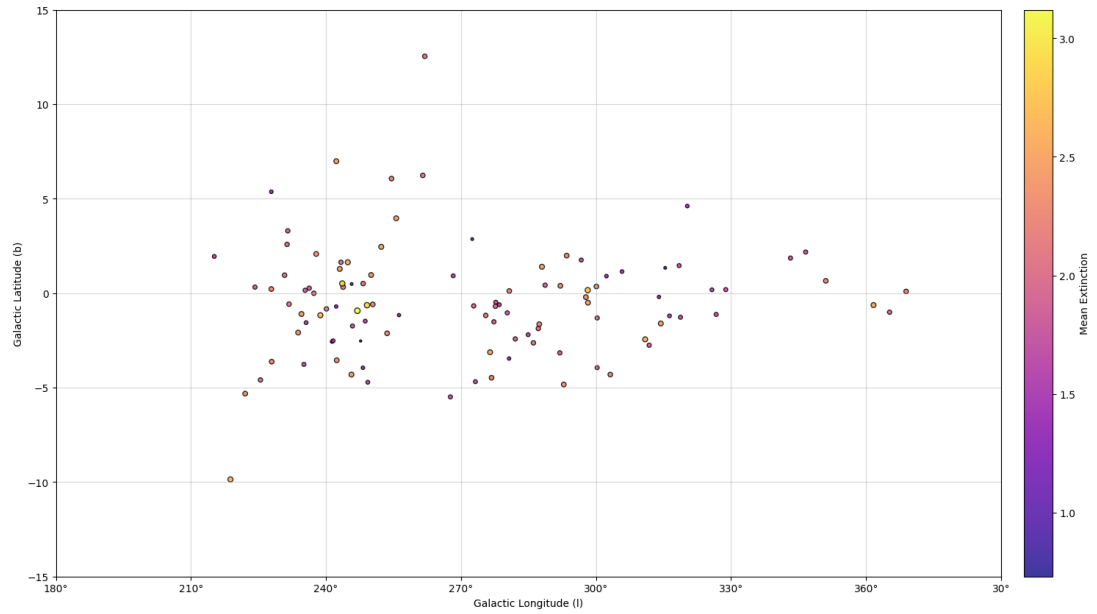


Figure 3.21: Sky distribution of 105 Galactic open clusters we used for the further analysis in this work.

## 4. Summary And Prospects

We will be able to carefully investigate known Galactic open clusters due to the Gaia Data Release 3. After gathering the available astrometric and photometric data, we uniformly observe 105 open clusters in the ultraviolet region using the DK1.54 and CASLEO telescopes.

### Our Goals Are As Follows:

1) Are the cluster candidates we observed with the DK1.54 and CASLEO telescopes real open clusters or not?

The answer to this question is the following:

We cross-match our UV data with Gaia DR3, then find the membership from the Hunt & Reffert (2023) catalogue based on the Gaia DR3 data, and then see that all clusters have membership and name in Hunt & Reffert catalogue. Hence, they are not new clusters and have already been identified.

2) Calculate the extinction for every cluster we observed across all passbands.

3) These data can be used to create the first homogeneous census of unexplored open clusters in the Milky Way using ultraviolet photometry. Min, Max, Median, Mean, and Mean Uncertainty tables for each of the 105 clusters in the various passbands are shown below.

Below are tables of Min, Max, Median, Mean, and Mean Uncertainty of all 105 clusters in different passbands.

Table 4.1: Min, Max, Median, Mean, and Mean Uncertainty of the  $E(U-BP)/E(BP-RP)$ .

Min $E(U-BP)$ $/E(BP-RP)$	Max $E(U-BP)$ $/E(BP-RP)$	Median $E(U-BP)$ $/E(BP-RP)$	Mean $E(U-BP)$ $/E(BP-RP)$	Mean Unc. $E(U-BP)$ $/E(BP-RP)$
0.02	2.11	0.97	0.97	0.24

Table 4.2: Min, Max, Median, Mean, and Mean Uncertainty of the  $E(U-G)/E(BP-RP)$ .

Min $E(U-G)$ $/E(BP-RP)$	Max $E(U-G)$ $/E(BP-RP)$	Median $E(U-G)$ $/E(BP-RP)$	Mean $E(U-G)$ $/E(BP-RP)$	Mean Unc. $E(U-G)$ $/E(BP-RP)$
0.46	2.47	1.38	1.40	0.24

Table 4.5: Min, Max, Median, Mean, and Mean Uncertainty of the  $E(U-G)/E(BP-G)$ .

Min $E(U-G)$ / $E(BP-G)$	Max $E(U-G)$ / $E(BP-G)$	Median $E(U-G)$ / $E(BP-G)$	Mean $E(U-G)$ / $E(BP-G)$	Mean Unc. $E(U-G)$ / $E(BP-G)$
1.10	5.35	3.29	3.28	0.52

Table 4.3: Min, Max, Median, Mean, and Mean Uncertainty of the  $E(U-RP)/E(BP-RP)$ .

Min $E(U-RP)$ / $E(BP-RP)$	Max $E(U-RP)$ / $E(BP-RP)$	Median $E(U-RP)$ / $E(BP-RP)$	Mean $E(U-RP)$ / $E(BP-RP)$	Mean Unc. $E(U-RP)$ / $E(BP-RP)$
1.02	2.95	1.98	1.98	0.22

Table 4.4: Min, Max, Median, Mean, and Mean Uncertainty of the  $E(U-G)/E(G-RP)$ .

Min $E(U-G)$ / $E(G-RP)$	Max $E(U-G)$ / $E(G-RP)$	Median $E(U-G)$ / $E(G-RP)$	Mean $E(U-G)$ / $E(G-RP)$	Mean Unc. $E(U-G)$ / $E(G-RP)$
1.05	4.03	2.36	2.39	0.50

Below are plots of different extinction ratios vs. distance (kpc).

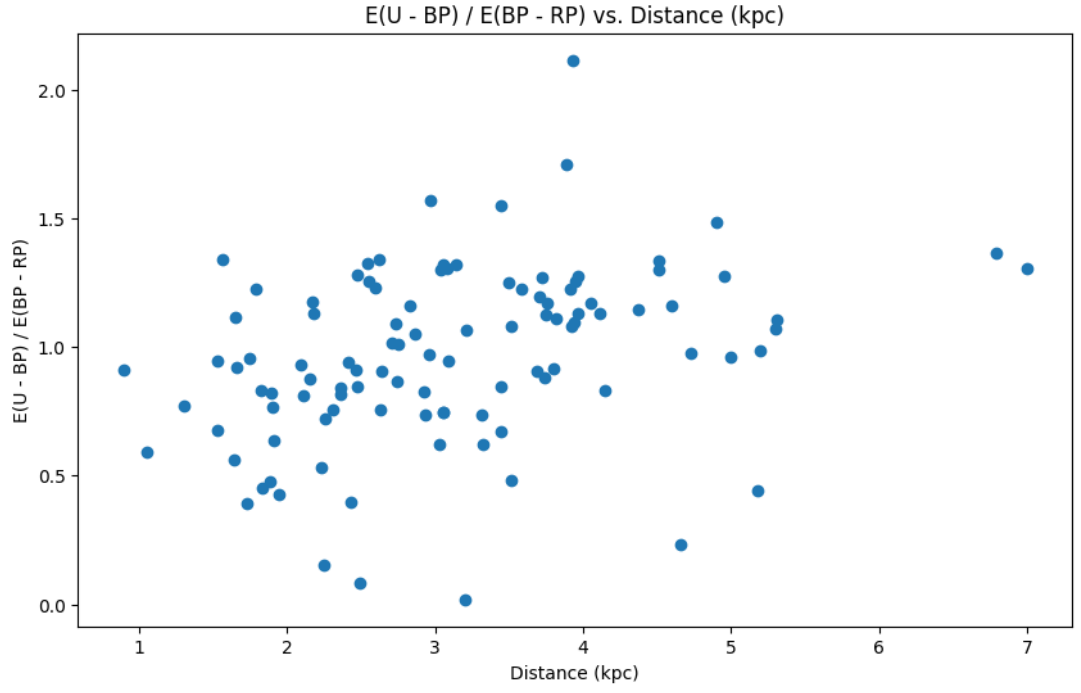


Figure 4.1:  $E(U-BP)/E(BP-RP)$  vs. Distance (kpc).

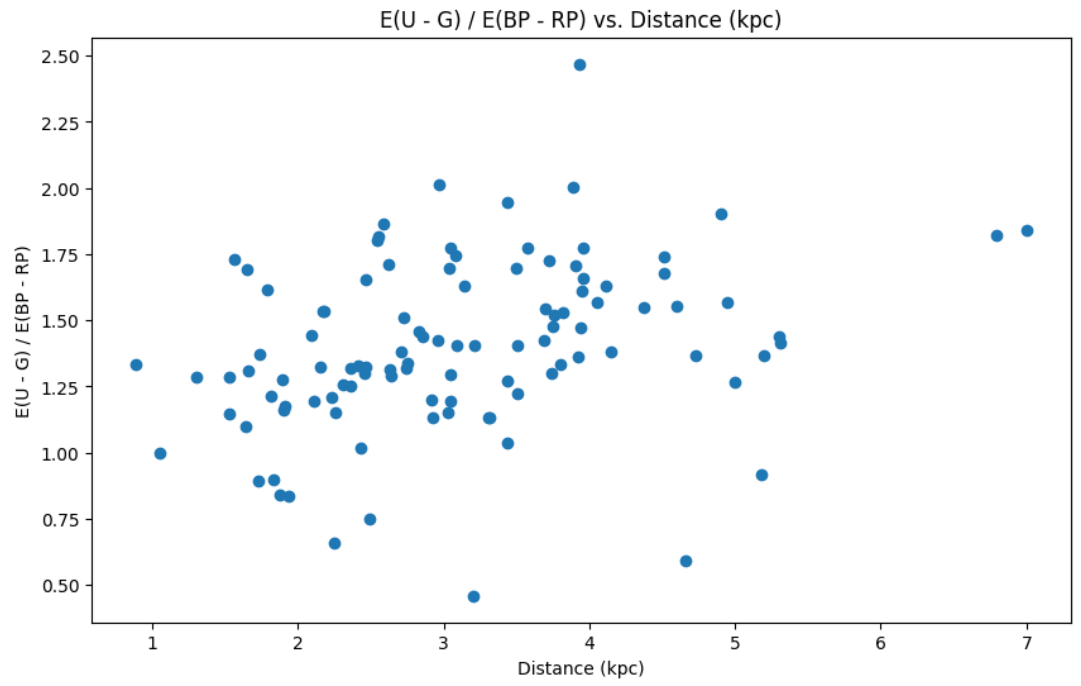


Figure 4.2:  $E(U-G)/E(BP-RP)$  vs. Distance (kpc).



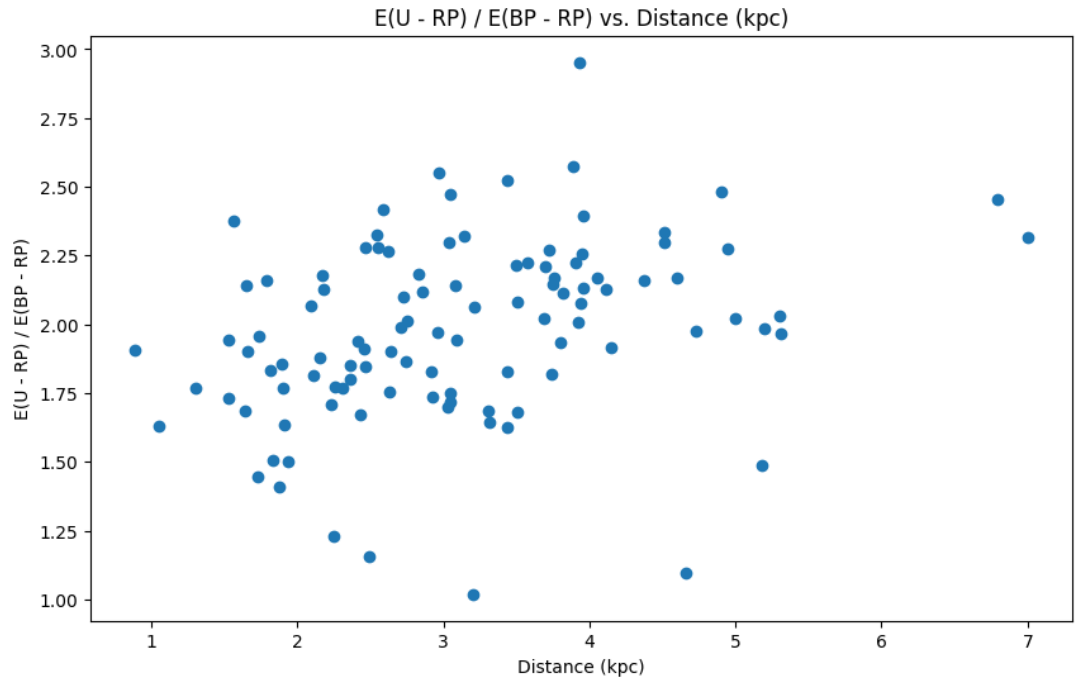


Figure 4.3:  $E(U-RP)/E(BP-RP)$  vs. Distance (kpc).

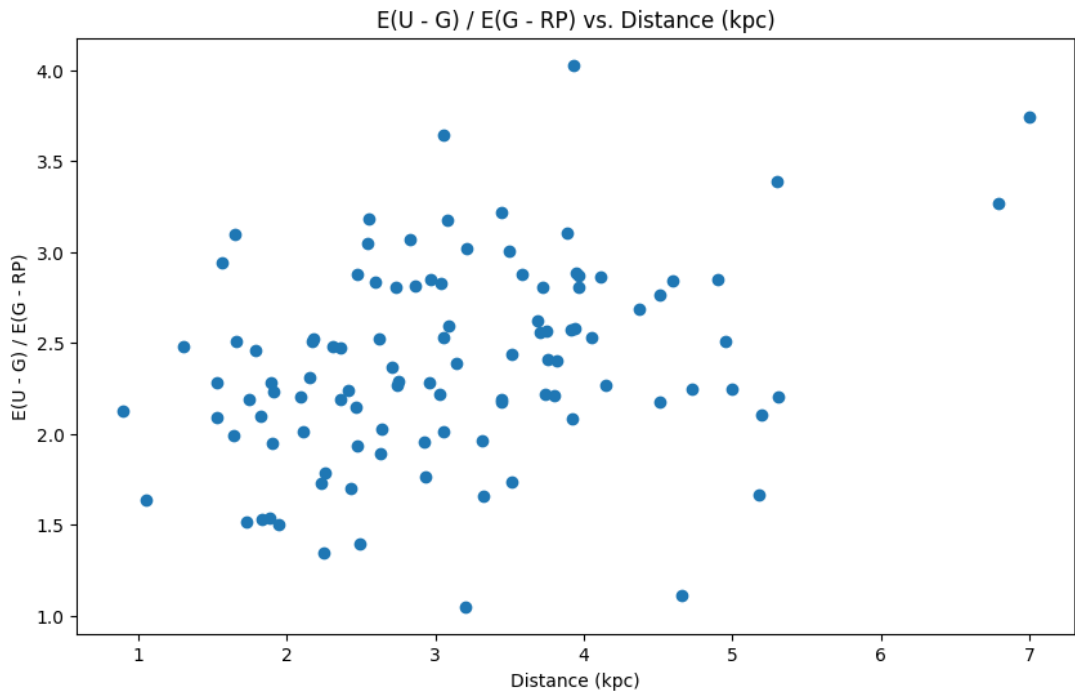


Figure 4.4:  $E(U-G)/E(G-RP)$  vs. Distance (kpc).

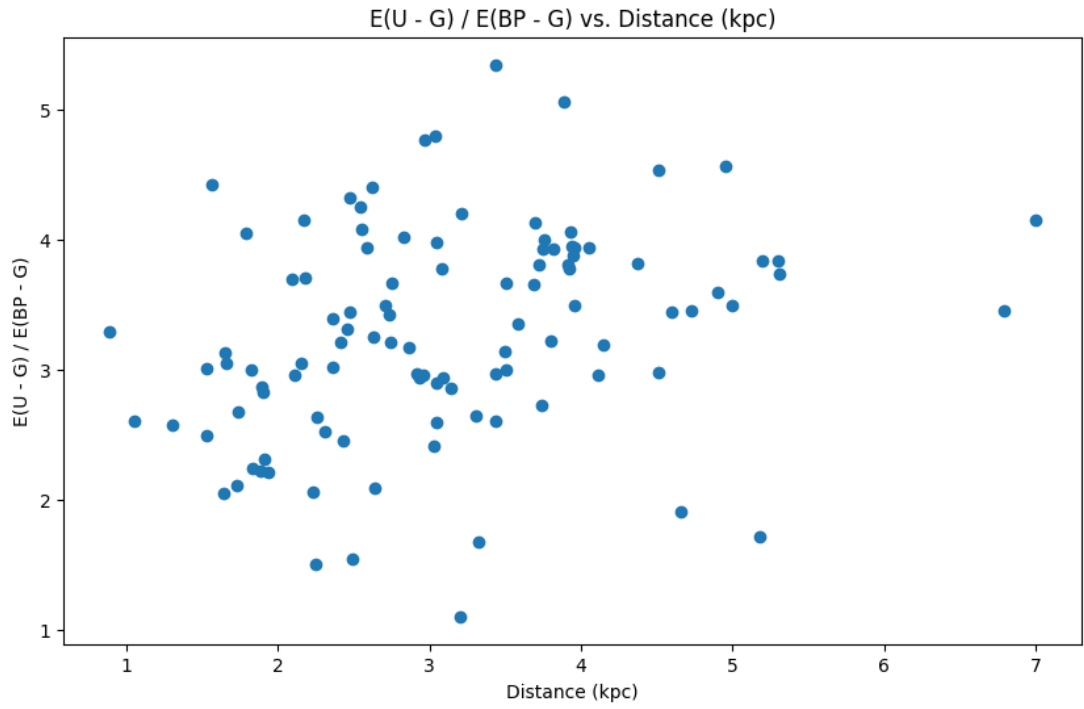


Figure 4.5:  $E(U-G)/E(BP-G)$  vs. Distance (kpc).

Below are the plots of different extinction ratios vs. log age (yr).

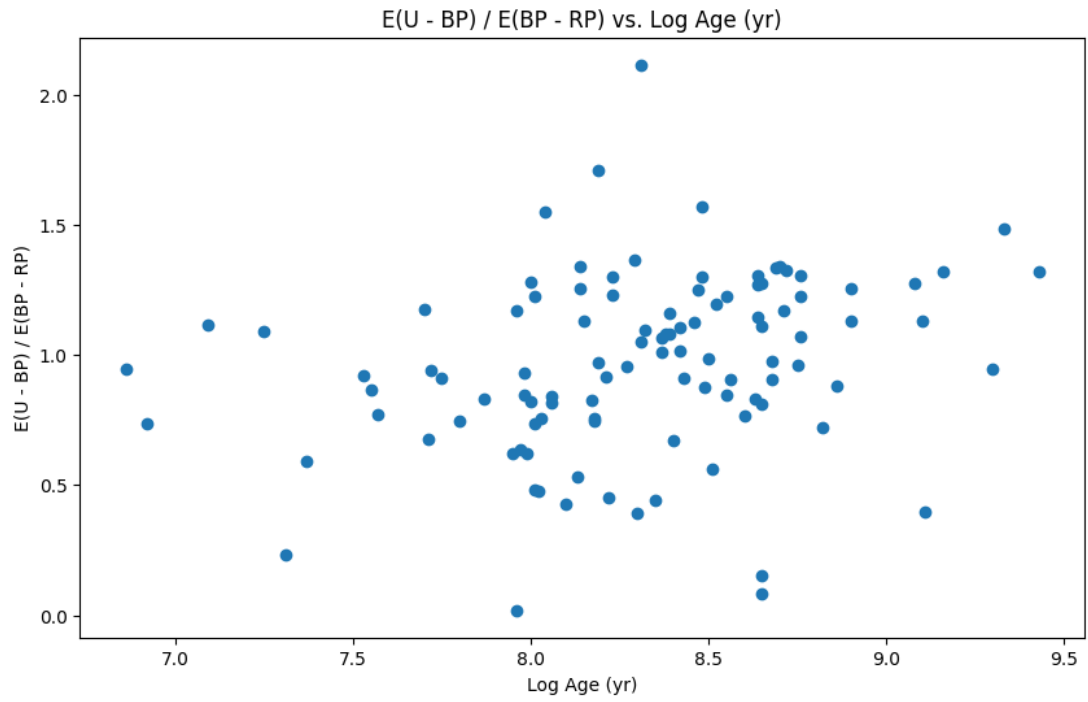


Figure 4.6:  $E(U-BP)/E(BP-RP)$  vs. Log Age (yr).

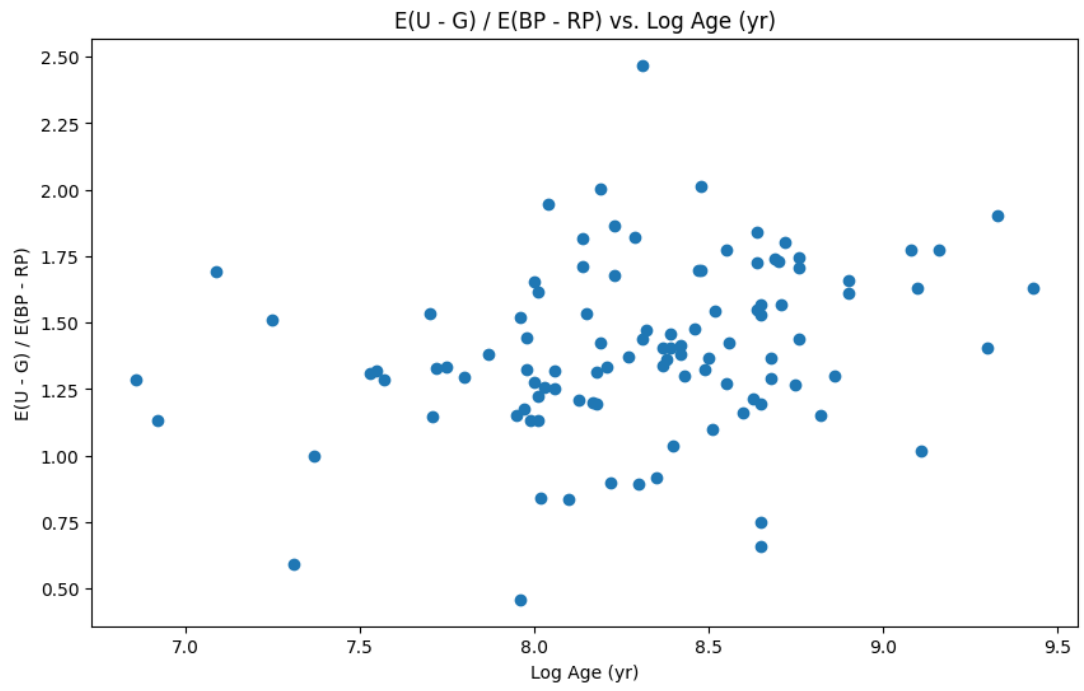


Figure 4.7:  $E(U-G)/E(BP-RP)$  vs. Log Age (yr).

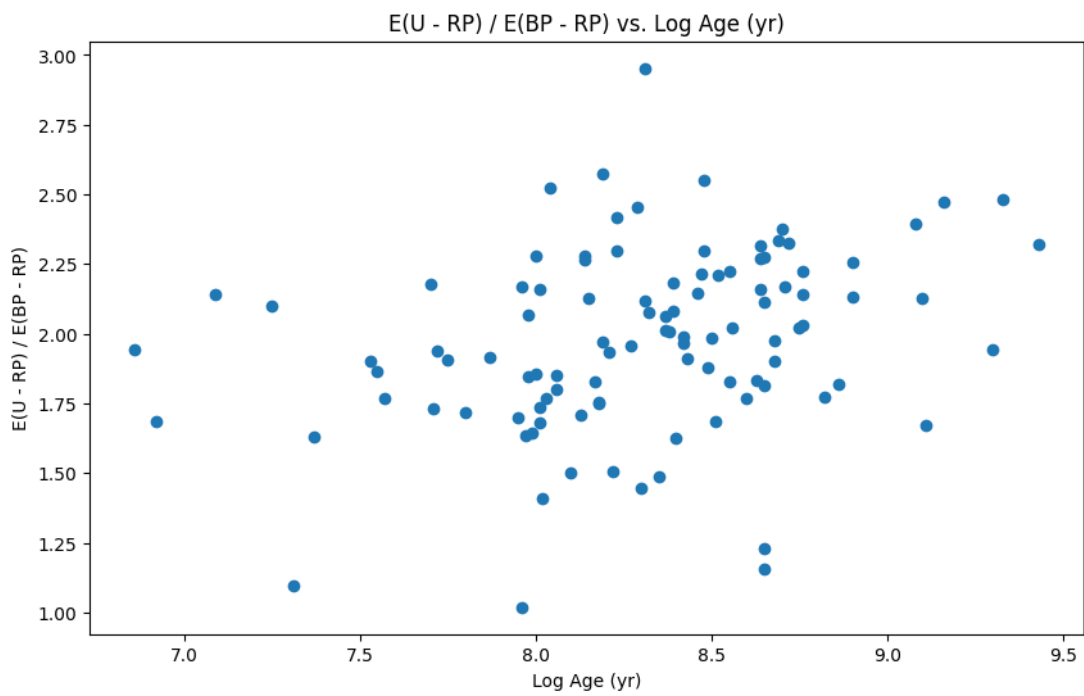


Figure 4.8:  $E(U-RP)/E(BP-RP)$  vs. Log Age (yr).

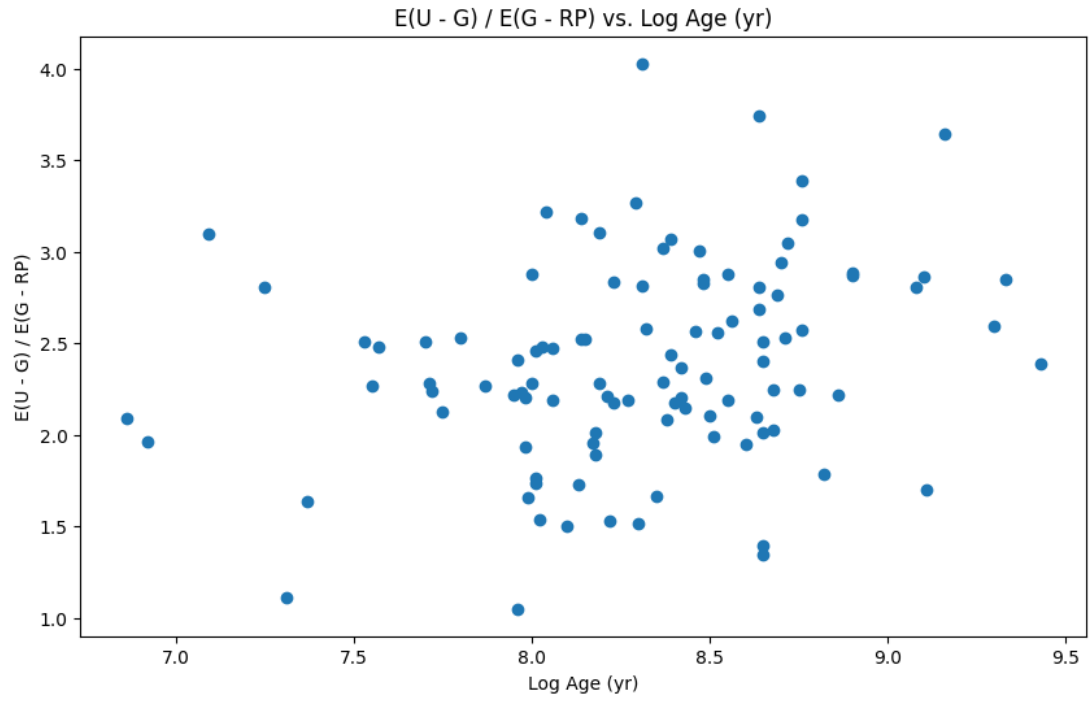


Figure 4.9:  $E(U-G)/E(G-RP)$  vs. Log Age (yr).

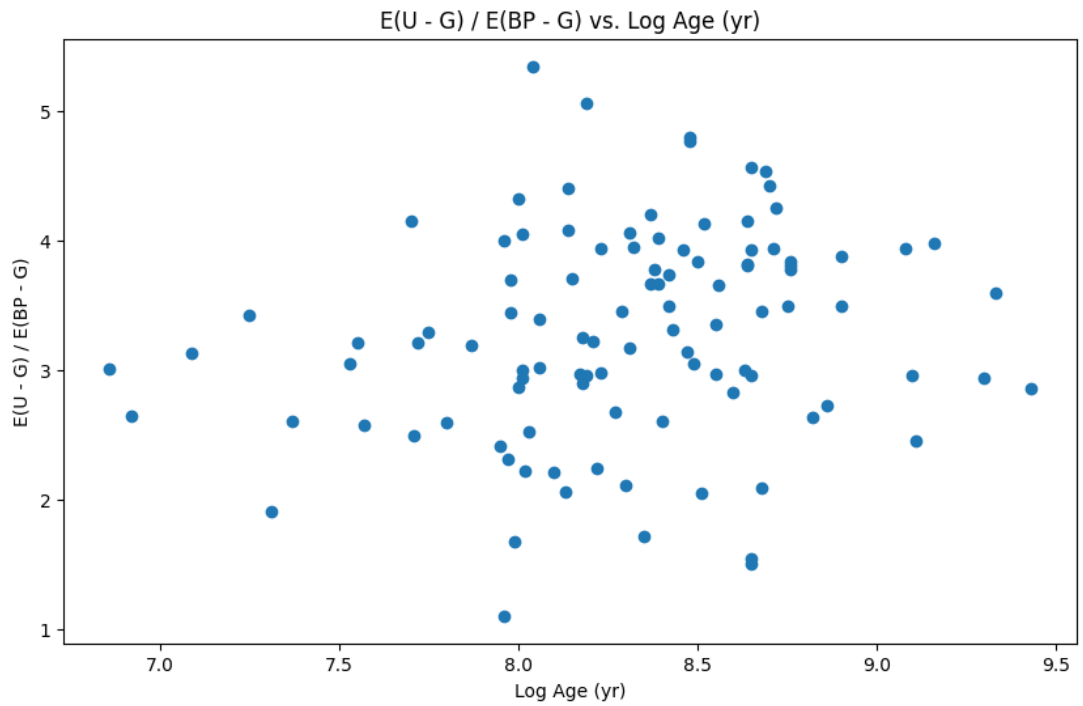


Figure 4.10:  $E(U-G)/E(BP-G)$  vs. Log Age (yr).

Stars in galaxies are born in molecular clouds (MCs), and the production of these clouds is complicated. The gravitational collapse of the dense regions in the interstellar medium of galaxies is an important mechanism (Keilmann et al. 2024).

Dust is made up of heavy elements resulting from star nuclear burning. Dust grains are formed by reprocessing these heavy elements in the interstellar medium after they are expelled from stars by winds and explosions (Draine 2003).

Dust significantly affects light propagation, scattering, and absorbing photons from ultraviolet to infrared wavelengths, leading to extinction and reddening effects in astronomical observations (Schlafly & Finkbeiner 2011).

There are two different effects of extinction:

1) Molecular cloud that the star cluster is born from, 2) Interstellar medium between observer and star cluster.

If the cluster is farther from the observer, there is more dust and gas between the observer and the star cluster. Therefore, the extinction is higher.

If the cluster is in the Galactic disk, then there is more dust and gas in the Galactic disk, so the cluster has additional extinction.

Stars in young clusters still have dust and gas (material) surrounding them because of differential extinction caused by the local environment within the one-star cluster. Therefore, the extinction is higher.

But in old clusters, stars already accreted dust and gas (material) from the molecular cloud, so they have less extinction.

### **Future Prospects Are As Follows:**

1) We would like to use the same processes for the northern hemisphere clusters we have observed to calculate their reddening.

2) Observe more clusters and have a catalogue of reddening for all our observed clusters.

# Bibliography

- Aballay, J. L., Cellone, S. A., Fernández, G. E. L., et al. 2019, Boletín de la Asociación Argentina de Astronomía La Plata Argentina, 61, 249
- Andersen, M. I. 2019, in The La Silla Observatory - From the Inauguration to the Future, 1
- Archinal, B. A. & Hynes, S. J. 2003, Star Clusters (Willmann-Bell)
- Bastian, N. & Lardo, C. 2018, Annual Review of Astronomy & Astrophysics, 56, 83
- Bessell, M. S. 2005, Annual Review of Astronomy & Astrophysics, 43, 293
- Bressan, A., Marigo, P., Girardi, L., et al. 2012, Monthly Notices of the Royal Astronomical Society, 427, 127
- Brown, A. G., Vallenari, A., Prusti, T., et al. 2018, EDP Sciences, 616
- Burkert, A. & Tremaine, S. 2010, The Astrophysical Journal, 720, 516
- Calabretta, M. R. & Greisen, E. W. 2002, Astronomy & Astrophysics, 395, 1077
- Canterna, R. 1976, Astronomical Journal, 81, 228
- Cardelli, J. A., Clayton, G. C., & Mathis, J. S. 1989, Astrophysical Journal, 345, 245
- Cárdenas, P. A., Martínez, M., Molina, M. G., & Mercado, P. E. 2023, Sustainability, 15, 15195
- ClabonWalter, A. & Cox, A. N. 2000, Allen's Astrophysical Quantities (Springer Science and Business Media)
- Draine, B. T. 2003, Annual Review of Astronomy & Astrophysics, 41, 241
- Fitzpatrick, E. L. 1999, The Publications of the Astronomical Society of the Pacific, 111, 63
- Fruchter, A. S. & Hook, R. N. 2002, The Publications of the Astronomical Society of the Pacific, 114, 144
- Fukugita, M., Ichikawa, T., Gunn, J. E., et al. 1996, Astronomical Journal, 111, 1748
- Gaia Collaboration, Brown, A. G. A., Vallenari, A., et al. 2016, Astronomy & Astrophysics, 595, A2
- Gaia Collaboration, Brown, A. G. A., Vallenari, A., et al. 2018, Astronomy & Astrophysics, 616, A1
- Gaia Collaboration, Brown, A. G. A., Vallenari, A., et al. 2021, Astronomy & Astrophysics, 649, A1

- Gaia Collaboration, Vallenari, A., Brown, A. G. A., et al. 2023, *Astronomy & Astrophysics*, 674, A1
- Gómez de Castro, A. I. & Wamsteker, W. 2004, *Lecture Notes and Essays in Astrophysics*, 1, 197
- Gratton, R., Bragaglia, A., Carretta, E., et al. 2019, *The Astronomy & Astrophysics Review*, 27, 8
- Grisetti, R. 2006, *A Student's Guide to CCD Photometry Data Processing using IRAF* (Springer Science and Business Media)
- Heasley, J. N. 1999, in *Astronomical Society of the Pacific Conference Series*, Vol. 189, *Precision CCD Photometry*, ed. E. R. Craine, D. L. Crawford, & R. A. Tucker, 56
- Hills, J. G. 1980, *Astrophysical Journal*, 235, 986
- Horne, K. 1986, *Publications of the Astronomical Society of the Pacific*, 98, 609
- Howell, S. B. 2006, *Handbook of CCD Astronomy* (Cambridge University Press)
- Hunt, E. L. & Reffert, S. 2023, *Astronomy & Astrophysics*, 673, A114
- Johnson, H. L. & Morgan, W. W. 1953, *Astrophysical Journal*, 117, 313
- Jordi, C., Gebran, M., Carrasco, J. M., et al. 2010, *Astronomy & Astrophysics*, 523, A48
- Keilmann, E., Kabanovic, S., Schneider, N., et al. 2024, *Astronomy & Astrophysics*, 692, A226
- Kerr, J. B. 2005, *Optical Engineering*, 44, 041002
- Kim, S.-H., Martin, P. G., & Hendry, P. D. 1994, *Astrophysical Journal*, 422, 164
- Lada, C. J. 2010, *Philosophical Transactions of the Royal Society of London Series A*, 368, 713
- Lee, E. S. & Forthofer, R. N. 2006, *Strategies for Variance Estimation* (SAGE)
- Leonard, P. J. T. 1989, *Astronomical Journal*, 98, 217
- Majidi, F. Z., Bradley, L., Ma, S., et al. 2024, in *EAS2024, European Astronomical Society Annual Meeting*, 236
- Monti, L., Muraveva, T., Clementini, G., & Garofalo, A. 2024, *Sensors*, 24, 5203
- Payne-Gaposchkin, C. 1979, *Stars and clusters* (Cambridge: Harvard University Press)
- Schlafly, E. F. & Finkbeiner, D. P. 2011, *The Astrophysical Journal*, 737, 103
- Shu, F. H., Adams, F. C., & Lizano, S. 1987, *Annual Rev. Astron. Astrophys.*, 25, 23

- Stetson, P. B. 1987, Publications of the Astronomical Society of the Pacific, 99, 191
- Stetson, P. B., Vandenberg, D. A., & Bolte, M. 1996, Publications of the Astronomical Society of the Pacific, 108, 560
- Strömgren, B. 1966, Annual Review of Astronomy & Astrophysics, 4, 433
- Sung, H., Lim, B., Bessell, M. S., et al. 2013, Journal of Korean Astronomical Society, 46, 103
- Tody, D. 1986, in Society of Photo-Optical Instrumentation Engineers (SPIE) Conference Series, Vol. 627, Instrumentation in astronomy VI, ed. D. L. Crawford, 733
- Valdes, F. G., Campusano, L. E., Velasquez, J. D., & Stetson, P. B. 1995, Publications of the Astronomical Society of the Pacific, 107, 1119
- Werner, N., Řípa, J., Münz, F., et al. 2022, in Society of Photo-Optical Instrumentation Engineers (SPIE) Conference Series, Vol. 12181, Space Telescopes and Instrumentation 2022: Ultraviolet to Gamma Ray, ed. J.-W. A. den Herder, S. Nikzad, & K. Nakazawa, 121810B
- Werner, N., Řípa, J., Thöne, C., et al. 2024, Space Science Reviews, 220, 11